UNIVERSITY OF GENOA

POLYTECHNIC SCHOOL

Department of Electrical, Electronic, Telecommunications Engineering, and Naval Architecture (DITEN)

Master's degree in Internet and Multimedia Engineering

THESIS

EXPERIMENTAL CALIBRATION OF GPR S-PARAMETER DATA FOR SUBSURFACE PROSPECTING

Supervisors: Prof. **Alessandro Fedeli**, Prof. **Andrea Randazzo**

Co-supervisor: Dr. **Valentina Schenone**

Candidate: **Eduardo Gómez González**

June 30th, 2023

Academic year 2022 – 2023

EXPERIMENTAL CALIBRATION OF GPR S-PARAMETER DATA FOR SUBSURFACE PROSPECTING

Abstract

The use of GPR imaging techniques is of great interest in certain fields such as archaeology, civil engineering or geology. However, in order to obtain results, an inverse problem needs to be solved. When working with experimental data, it is necessary to adopt calibration techniques due to the spurious effects that appear. For this reason, two antenna calibration methods have been implemented and evaluated in this thesis with several test and calibration targets, obtaining results that will be beneficial for current and to continue with future research in this field. The activities related to this thesis have been carried out at the Applied Electromagnetics Laboratory of the Department of Electrical, Electronic, Telecommunication Engineering, and Naval Architecture (DITEN) of the University of Genoa.

Keywords: Ground Penetrating Radar, GPR imaging, S-parameter calibration, Subsurface prospecting.

Summary

Table of Figures

Table of Tables

Chapter 1
Introduction

1.1 Introduction to GPR techniques for subsurface inspection

Ground Penetrating Radar (GPR) is a non-destructive geophysical technique used to inspect subsurface structures and features. It provides information about the composition, depth and spatial distribution of materials beneath the surface. GPR systems are widely adopted in various fields such as archaeology, geology or civil engineering. [1] [2]

The principle of operation of this technique consists in the transmission and reception of electromagnetic waves over the region to be inspected. In order to penetrate the subsurface, frequencies from 10 MHz up to several GHz are used. As waves propagate through the different subsoil materials different reflection and scattering processes are produced, therefore, by analysing the characteristics of these signals, different information about the underground region can be obtained. [3]

The main advantage of this procedure is its non-invasiveness, which is a key element compared to classical methods that require excavations. This places it as a useful alternative in scenarios where the preservation of structural integrity and the non-disturbance of the surrounding environment are essential.

The output of the GPR systems is commonly given as a B-scan, which consists of the two-dimensional representation of the amplitude of the waves received with respect to the instant of reception and the position in which the measurement has been taken. A B-scan can also be understood as the grouping of several A-scans obtained at different positions, which are a representation of the amplitude of the received wave versus time.

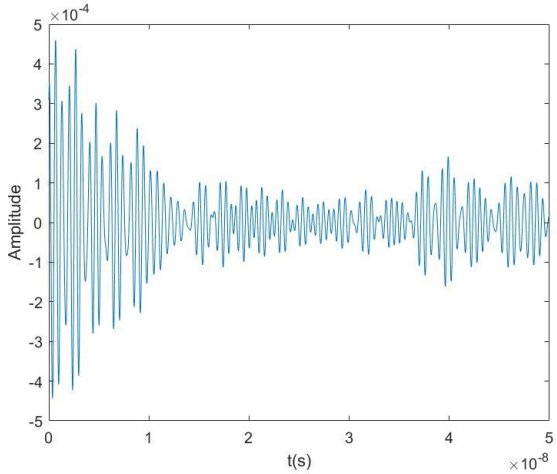

Figure 1.1. A-scan example

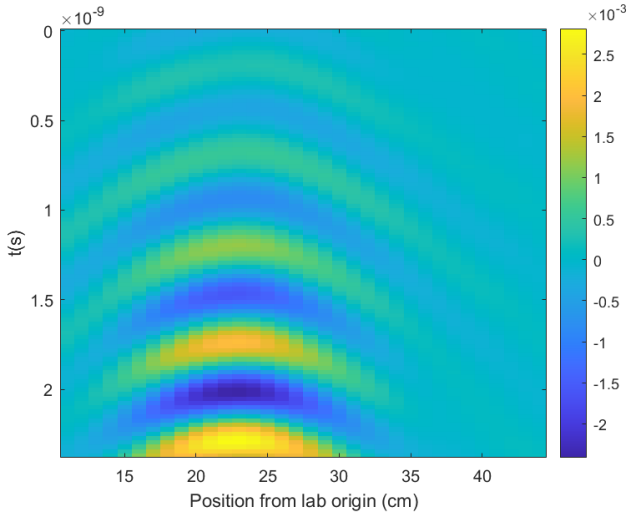

Figure 1.2. B-scan example

Nevertheless, the interpretation of these data is complex and requires specialist users with knowledge in understanding the characteristics of different subsurface materials and the behaviour of electromagnetic waves.

Therefore, the inverse-scattering methods entail a significant improvement by giving a direct representation of the dielectric properties of the region inspected by processing the measured data. [1]

1.2 Formulation of the problem

The working scenario is described in Figure 1.3, where three different regions are differentiated: air, which is modelled as vacuum ($\varepsilon_0 \approx 8.85 \times 10^{-12}\ F/m$); soil, which is characterized by a complex relative dielectric permittivity ε_b and, inside it, the Investigation domain *R*, where targets are considered to be located. The boundary between air and sand is defined with the letter Λ. This representation is a two-dimensional section of the tri-dimensional real scenario.

It is assumed that the electromagnetic properties of the configuration do not change along z-axis, including the target. Moreover, the electromagnetic field is supposed to be transverse-magnetic to z-axis, hence the electric field only variates in x and y directions. With these two assumptions, the electromagnetic problem becomes scalar and two-dimensional [1].

In this case, a monostatic configuration with one waveguide antenna positioned at height h from air-soil interface, parallel to x-axis is proposed. Therefore, this antenna is used for both transmission and reception. The parameter evaluated in the antenna port is S_{11}, which relates the returned and emitted signals. Measurements of this parameter are done in Q distinct positions, denoted by the index $q = 1,2,\dots,Q$ along the line of length l_m and at F different frequencies, identified by the index $f = 1,2,\dots,F$. Consequently, we define parameters ${S_{11,TOT}}^{q,f}$ and ${S_{11,INC}}^{q,f}$ which are, respectively, the values with and without the presence of the target in the investigation domain. Since in a practical case it is impossible to obtain ${S_{11,INC}}^{q,f}$, we can estimate it. Therefore, the difference between these two parameters is defined, and from now on will be referred to as the scattered field:

$$\delta {S_{11}}^{q,f} = {S_{11,TOT}}^{q,f} - {S_{11,INC}}^{q,f} \tag{1.1}$$

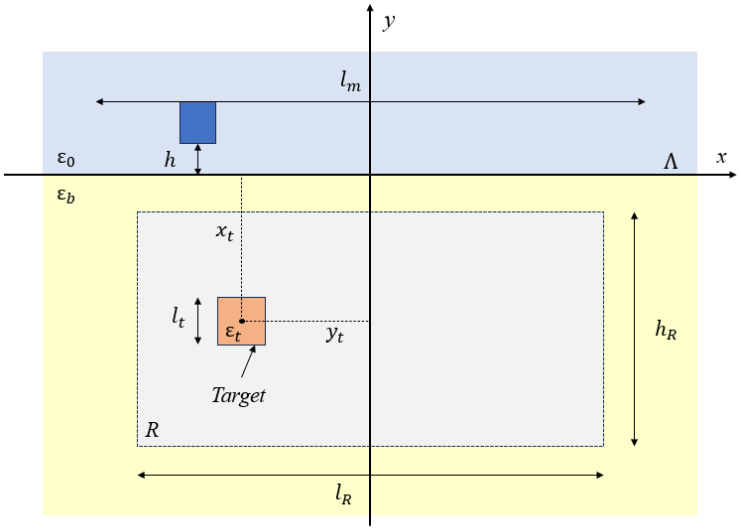

Figure 1.3. Working scenario

The main objective is to find the dielectric permittivity inside the region R, $\varepsilon(x, y)$ in order to study its dielectric properties. Therefore, the contrast function can be defined as:

$$\tau(x, y) = \frac{\varepsilon(x, y) - \varepsilon_b}{\varepsilon_b} \tag{1.2}$$

It can be proven that, in a two-dimensional setting, contrast function is related with scattering parameters by (1.3) equation. [4]

$$\delta S_{11}{}^{q,f} = -\frac{j\omega\varepsilon_b}{2c^2} \iint_R E_{inc}^{q,f}(x, y) E_{tot}^{q,f}(x, y) \tau(x, y)\, dxdy \tag{1.3}$$

where $E_{tot}^{q,f}$ and $E_{inc}^{q,f}$ are, respectively, the electric field with and without the presence of the target inside R for antenna position q and frequency f. Consequently, as both $E_{tot}^{q,f}$ and $\tau(x, y)$ depend on the properties on the target, the problem is nonlinear since two unknown values are multiplied. Moreover, the relation is ill-posed because if we slightly change $\delta S_{11}{}^{q,f}$ we obtain very different values of $\tau(x, y)$.

Combining all the available data (i.e., different frequencies and positions), the (1.4) system of equations is obtained.

$$\bar{b} \triangleq \begin{bmatrix} \delta S_{11}{}^{1,1} \\ \vdots \\ \delta S_{11}{}^{Q,F} \end{bmatrix} = \begin{bmatrix} -\frac{j\omega\varepsilon_b}{2c^2} \iint_R E_{inc}^{q,f}(x,y) E_{tot}^{q,f}(x,y) \tau(x,y)\, dxdy^{1,1} \\ \vdots \\ -\frac{j\omega\varepsilon_b}{2c^2} \iint_R E_{inc}^{q,f}(x,y) E_{tot}^{q,f}(x,y) \tau(x,y)\, dxdy^{Q,F} \end{bmatrix} \triangleq \bar{N}(\tau) \qquad (1.4)$$

In order to solve (1.4) and retrieve $\varepsilon(x,y),\ (x,y) \in R$, inverse-scattering procedures can be applied. [5]–[15]

1.3 Justification on calibration necessity

As explained before, the main purpose of this thesis is to evaluate the two calibration methods proposed in Sections 2.1.1 and 2.1.2, therefore the first step is to obtain S_{11} coefficients from the waveguide antenna of equation (1.4).

Measures are acquired inside the Applied Electromagnetics Laboratory; thus, spurious contributions of the antenna, antenna port and surroundings affect the parameters obtained. Consequently, in order to obtain real S_{11} values without the mentioned contributions, an antenna calibration procedure developed by S.Lambot *et al.* [16] is followed to match between simulation and experimental cases. Otherwise, since the antenna and antenna port cannot be modelled in a perfect way within the inversion method, it cannot be employed to obtain results.

Chapter 2
Development

2.1 Calibration method

The procedure followed has been proposed in [16]. It is defined for a monostatic configuration in which S_{11} coefficients are measured using a Vector Network Analyzer (VNA). The VNA reference plane, where parameters are measured, is set at the connection between the VNA cable and the antenna port.

The antenna is modeled as a causal time-invariant linear system composed of different elementary blocks representing its transfer functions. First, the complex return loss, $H_i(\omega)$, represents the reflections that are present due to the variations of impedance between the antenna port, antenna cavity and air. Then, transmitting and receiving transfer functions, $H_t(\omega)$ and $H_r(\omega)$ respectively, model the antenna gain and phase delay between the measurement point and the source and receiver point. Feedback loss transfer function, $H_f(\omega)$, also describes different reflections between the antenna and the subsurface because of variations of impedance between the antenna feed point, aperture and air.

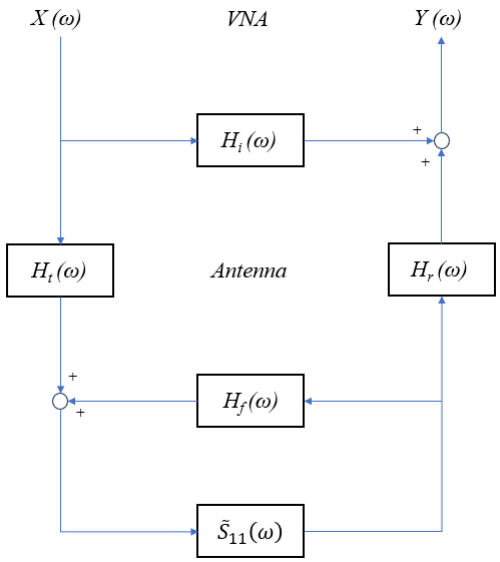

Figure 2.1. Block diagram representing the configuration

Figure 2.1 shows the block diagram used to model the configuration, where $Y(\omega)$ and $X(\omega)$ are the received and emitted signals at the VNA reference plane; $H_i(\omega)$, $H_t(\omega)$, $H_r(\omega)$ and $H_f(\omega)$ are, respectively, the complex return loss, transmitting, receiving, and feedback loss transfer functions of the antenna. Consequently, defining $S_{11}(\omega)$ as the complex ratio between $Y(\omega)$ and $X(\omega)$ and $\tilde{S}_{11}(\omega)$ as the ratio without the spurious contributions, the transfer function specified in frequency domain is:

$$S_{11}(\omega) = \frac{Y(\omega)}{X(\omega)} = H_i(\omega) + \frac{H_r(\omega) \cdot H_t(\omega) \cdot \tilde{S}_{11}(\omega)}{1 - H_f(\omega) \cdot \tilde{S}_{11}(\omega)} \tag{2.1}$$

Moreover, defining $H(\omega) = H_r(\omega) \cdot H_t(\omega)$, the number of transfer functions to be determined is reduced to three:

$$S_{11}(\omega) = H_i(\omega) + \frac{H(\omega) \cdot \tilde{S}_{11}(\omega)}{1 - H_f(\omega) \cdot \tilde{S}_{11}(\omega)} \tag{2.2}$$

At this point, after finding the transfer functions, the following expression can be used to calibrate an independent set of measurements taken experimentally:

$$\tilde{S}_{11}(\omega) = \frac{S_{11}(\omega) - H_i(\omega)}{H_f(\omega) \cdot S_{11}(\omega) - H_f(\omega) \cdot H_i(\omega) + H(\omega)} \tag{2.3}$$

In order to obtain the mentioned transfer functions and be able to apply (2.3), two procedures are discussed and compared.

2.1.1 First option: Least squares solution of non-linear system

In this case, the strategy consists of performing a series of measurements at *Q* different positions, where *Q* must be greater than or equal to the number of unknowns, in this case the three transfer functions. In this way, a non-linear system of equations is defined. The mentioned system is composed of the following expressions, one for each value of *q*, where *q* denotes the position number in which the measure has been taken:

$$S_{11}^{q}(\omega) = H_i(\omega) + \frac{H(\omega) \cdot \tilde{S}_{11}^{q}(\omega)}{1 - H_f(\omega) \cdot \tilde{S}_{11}^{q}(\omega)} \tag{2.4}$$

In the expression above, $S_{11}^{q}(\omega)$ represents the experimental measure taken at position q, while $\widetilde{S}_{11}^{q}(\omega)$ refers to the theoretical calibrated value. As at this point the calibrated value is unknown, the latter is obtained by means of the simulation procedure explained in Section 2.2.2.

In order to solver the non-linear system of equations, the strategy followed consists of finding its least squares solution. With this aim, a MATLAB script has been developed and the function *lsqnonlin()* [17] has been used. This expression receives as input arguments the functions whose sum of squares is minimized, the non-linear system in this case, and the initial point or initial array of points in which the algorithm starts. In order to obtain the transfer functions at the different frequencies desired, the function is executed inside an iterative process for each frequency. In this case, denoting the unknowns as:

$$\begin{aligned} x_1 &= H(\omega) \\ x_2 &= H_i(\omega) \\ x_3 &= H_f(\omega) \end{aligned} \tag{2.5}$$

and, therefore, each one of the functions described in (2.4) as $f_q(x_1, x_2, x_3)$, the mentioned *lsqnonlin()* function searches on each iteration for the solution of this problem, at the corresponding frequency of the iteration, given an initial point (x_{01}, x_{02}, x_{03}):

$$\min_{(x_1,x_2,x_3)} (f_1(x_1, x_2, x_3)^2 + f_2(x_1, x_2, x_3)^2 + \ldots + f_Q(x_1, x_2, x_3)^2) \tag{2.6}$$

For more details on the code implemented, see Annex: Implemented code.

2.1.2 Second option: $H_i(\omega)$ as freespace transfer function

This case follows the strategy proposed in [16], where the return loss transfer function, $H_i(\omega)$, can be obtained measuring $S_{11}(\omega)$ parameter in freespace conditions, where $\tilde{S}_{11}(\omega) = 0$.

The procedure followed in order to obtain $H_i(\omega)$ consists in measuring $S_{11}(\omega)$ parameter of the antenna with it pointing towards a flat surface, such as a wall, at a distance of 4 metres. The signal is then temporarily gated until the instant when the reflection from the wall is received, simulating in this way, if the distance to the wall is enough, the temporal received signal in free space. This time, assuming the speed of propagation of electromagnetic waves as the speed in vacuum and a distance from the wall of 4 metres is: $t_w = 2 * d/c = 26{,}67\ ns$.

The following figure presents the temporal signal measured after performing the inverse fast Fourier transform to the obtained $S_{11}(\omega)$ coefficients and the temporal signal after the time gating up to $26{,}67\ ns$.

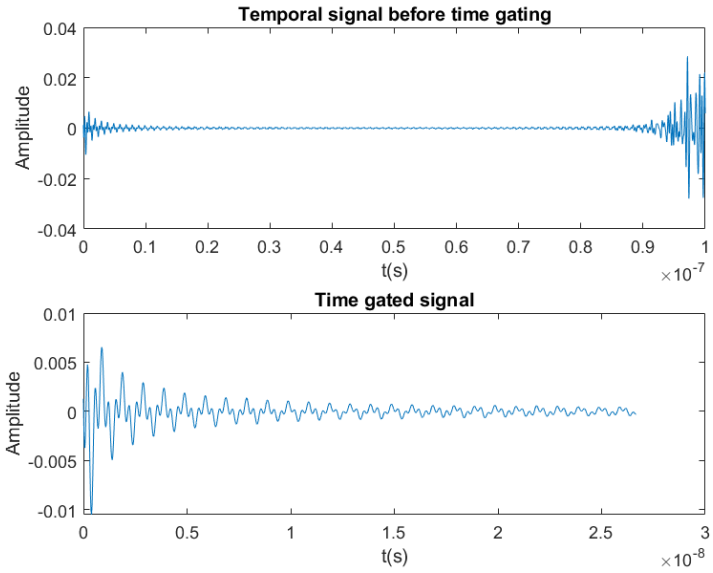

Figure 2.2 Temporal signals before and after time gating

After that, $H_i(\omega)$ is obtained as the fast Fourier transform of the time gated signal.

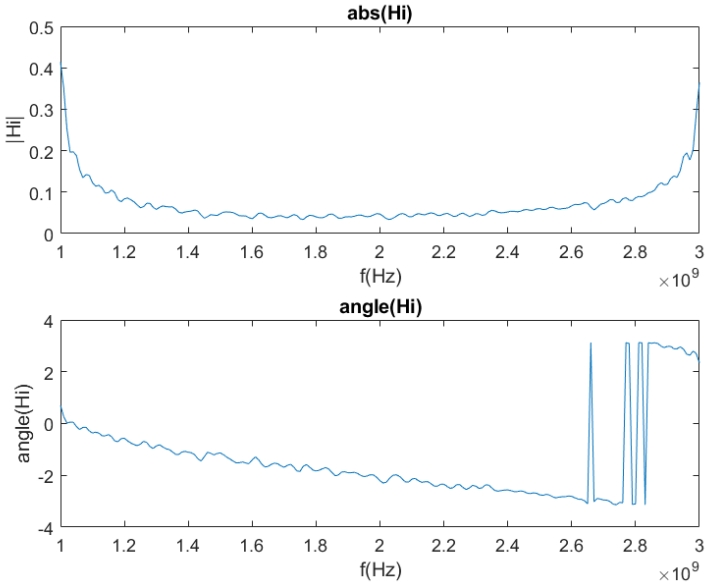

Figure 2.3 $H_i(\omega)$ obtained as freespace transfer funtion in range 1 GHz - 3 GHz

Then, as explained in Section 2.2.2.3, only the range from 1.45 GHz to 2 GHz is used. Therefore, the function in the mentioned frequencies is the following:

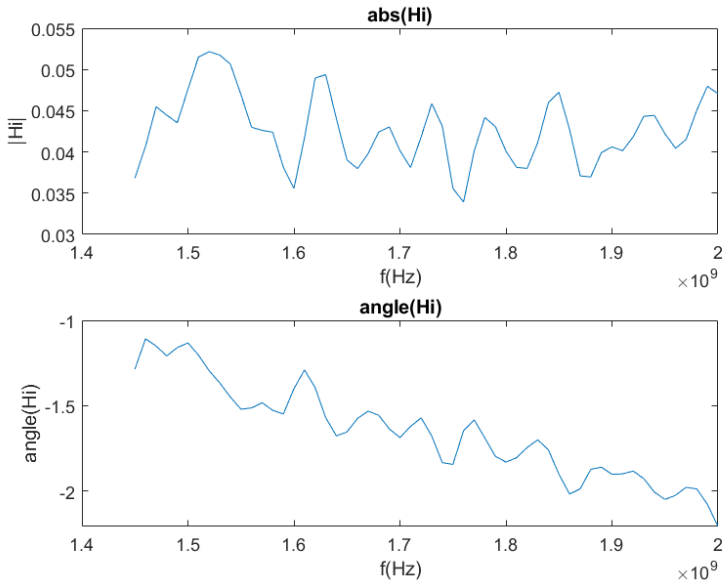

Figure 2.4 $H_i(\omega)$ in range 1.45 GHz - 2 GHz

At this point, known $H_i(\omega)$, the problem becomes linear and with two unknowns, and equation (2.2) can be expressed as follows:

$$\tilde{S}_{11}(\omega)\cdot\left(H_i(\omega)-S_{11}(\omega)\right)\cdot H_f(\omega)-\tilde{S}_{11}(\omega)\cdot H(\omega)=H_i(\omega)-S_{11}(\omega) \tag{2.7}$$

The strategy followed in [16] consists of realising two measures at different distances of a metal sheet, therefore there are two configurations and two measured values of $S_{11}(\omega)$. Regarding $\tilde{S}_{11}(\omega)$, the values for both configurations are computed. Thus, a linear system of two equations with two unknowns is defined and its solution is found for each frequency.

The procedure developed in this case is based on the previous, with the difference that instead of two configurations, *Q* are used and, rather than using various positions in front of a metal plate, positions are defined in front of several calibration targets, as presented in Sections 3.1.1, 3.2.1 and 3.3.1.

Therefore, defining, as it has been mentioned before, *Q* measures in different positions, $H(\omega)$ and $H_f(\omega)$ can be found by solving a system of equations based on expression (2.7) in a matrix form $\bar{A}\cdot\bar{x}=\bar{y}$, where the corresponding coefficients are:

$$\bar{A}=\begin{bmatrix}\tilde{S}_{11}{}^{1}(\omega)\cdot\left(H_i(\omega)-S_{11}{}^{1}(\omega)\right) & -\tilde{S}_{11}^{1}(\omega)\\ \vdots & \vdots\\ \tilde{S}_{11}{}^{Q}(\omega)\cdot\left(H_i(\omega)-S_{11}{}^{Q}(\omega)\right) & -\tilde{S}_{11}^{Q}(\omega)\end{bmatrix}$$

$$\bar{x}=\begin{bmatrix}H_f(\omega)\\ H(\omega)\end{bmatrix} \tag{2.8}$$

$$\bar{y}=\begin{bmatrix}H_i(\omega)-S_{11}^{1}(\omega)\\ \vdots\\ H_i(\omega)-S_{11}^{Q}(\omega)\end{bmatrix}$$

In order to solve it, first $\tilde{S}_{11}^{q}(\omega)$ values are computed by means of a simulation procedure presented in Section 2.2.2 and $S_{11}^{q}(\omega)$ data is acquired in the laboratory. Then, a MATLAB script has been developed, where the least squares solution for the linear system is obtained by means of *lsqr()* function [18] for each frequency. The mentioned function receives as input arguments the coefficients matrix $\bar{A}$ and the corresponding matrix of the right-hand

side of the equation $\bar{y}$ and finds the least squares solution for matrix $\bar{x}$ that minimizes $\|\bar{y} - \bar{A} \cdot \bar{x}\|$. This procedure is applied inside an iterative loop in order to obtain the desired transfer functions for frequencies each 10 MHz in the range 1.45 GHz – 2 GHz.

For more details on the code implemented see Annex: Implemented code.

2.2 Procedure for obtaining $S_{11}(\omega)$ and $\tilde{S}_{11}(\omega)$

In this section, techniques conducted in order to obtain both $S_{11}^{q}(\omega)$ and $\tilde{S}_{11}^{q}(\omega)$ values are explained. While the experimental values are measured at the Applied Electromagnetics Laboratory of the University of Genoa, the theoretical ones are obtained by means of simulations trying to accurately represent the existing scenario in the laboratory.

2.2.1 Experimental scenario

In Figure 2.5, the working environment where measures have been acquired is presented. There, the sand box in which the different targets are buried can be observed, as well as the metal plate placed under it, the waveguide antenna and the mechanism used to move it along the measurement line, named positioner. Moreover, the VNA with which measurements are obtained and the PC from where the data acquisition system is controlled are present in the mentioned figure.

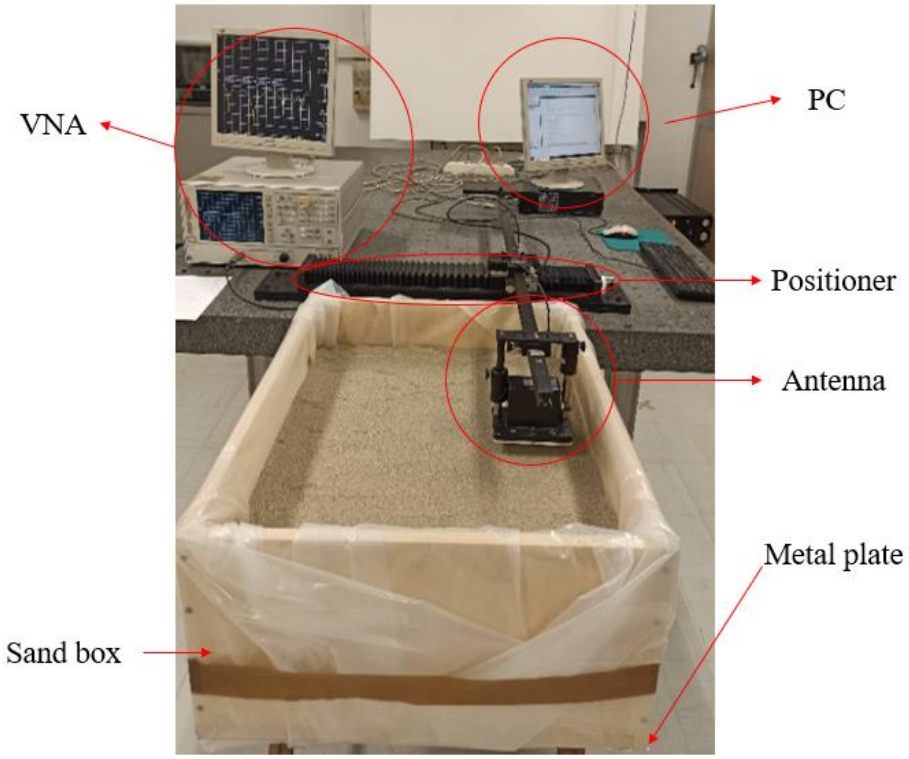

Figure 2.5. Laboratory Configuration

2.2.1.1 Instrumentation

The configuration proposed consists in a wood box filled with dry sand with relative dielectric permittivity $\varepsilon_r = 2.3384$, where targets are buried. An open-ended waveguide *WR240* antenna filled with dry sand is used to perform measurements and is located above the surface, leaving a separation of 3.5 cm in between. Moreover, a metal plate is located under the box in order to act as a perfect reflector.

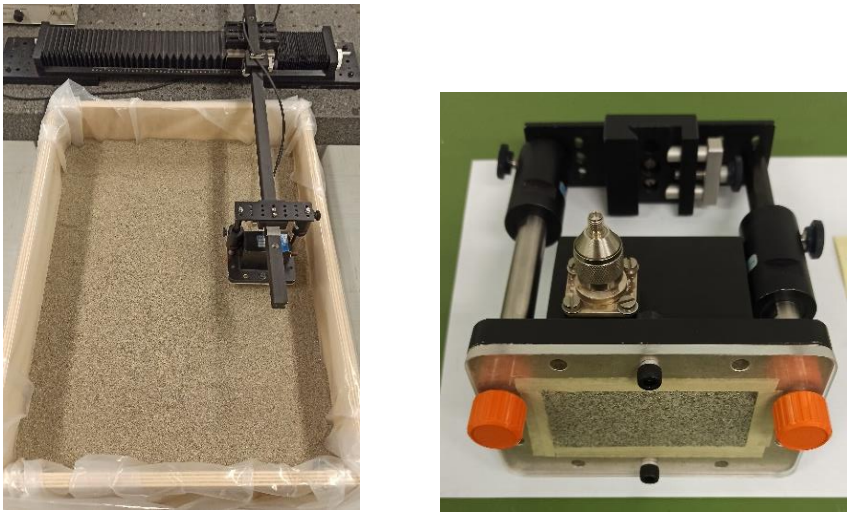

Figure 2.6. (a) Configuration of the sand box and the antenna. (b) Antenna used.

The antenna port is connected to a Vector Network Analyzer (VNA) in order to obtain $S_{11}(\omega)$ parameters on its port and, after that, these values are transferred to the computer using *.s1p file format. The VNA is configured to obtain data from 1 GHz to 3 GHz with a step of 10 MHz, however, only the range from 1.45 GHz to 2 GHz is used, according to Section 2.2.2.3.

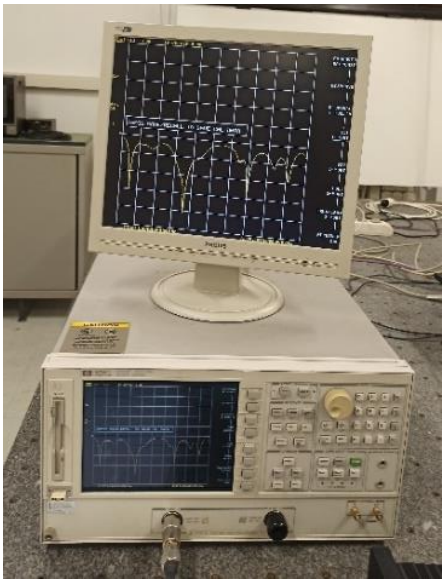

Figure 2.7. Vector Network Analyzer

2.2.1.2 Data acquisition

The first step when acquiring data is to calibrate the VNA: in order to do this, a 3.5 mm calibration kit from HP is used to establish the measurement reference plane at the connector between the cable and the antenna. As only one port is used, the technique followed is the so called short-open-load (SOL) calibration.

Figure 2.8. VNA calibration kit

Then, the antenna is moved along a line of length $l_m = 33\ cm$ with different step sizes, so measurements are obtained in Q positions. At each position, as the VNA is configured to measure from 1 GHz to 3 GHz with a step of 10 MHz, 201 S_{11} values are stored, one for each frequency. The communication and control of the VNA is done through MATLAB and Keysight I/O library.

Details on each specific measure carried out are given in Chapter 3.

2.2.2 Simulation scenario

The purpose of this step is to accurately simulate laboratory conditions so that the S_{11} parameters obtained can be used in the calibration method.

In order to achieve that, a numerical solver based on a finite-elements approach developed by the Applied Electromagnetics Group of the University of Genoa is used [5] and it is necessary to introduce the correct inputs to it: first, a description of the geometry of the problem is provided using the open-source program GMSH, which produces a .msh

file; then, physical parameters of the different materials are described, as well as the different frequencies and positions used. After that, all this information is introduced to the numerical solver, which generates S_{11} values at the waveguide port for each frequency and position using the standard format *.s1p. Thus, this data can be imported to MATLAB and used in the calibration process.

2.2.2.1 Geometry of the problem

As it has been mentioned before, GMSH is used, which is an open-source mesh generator that can be controlled by its graphical interface or from the command line. The different materials of the scenario are described along with its physical characteristics, they are also represented with different numbers in Figure 2.9 and detailed in Table 2.1. Moreover, an artificial material called PML (Perfect Matching Layer) is described surrounding the box in order to emulate free space boundary conditions, with the purpose of acting as an absorbing layer for electromagnetic waves.

In addition, a PEC (Perfect Electric Conductor) layer is defined under the wood box to simulate the metal plate placed in the real environment. Regarding the waveguide antenna, its side layers are defined as two plates of PEC and the waveguide port is defined at its upper part.

Table 2.1 Geometry file materials

Number	Material
4,13	Dry Sand
5,6,7	PMA/PML
8	Wood
9	Air

The different measurements that can be seen in Figure 2.9 represent the dimensions of the present elements and have been adjusted to the actual values of the laboratory setup. Table 2.2 shows their description as well as the obtained results.

Table 2.2 Geometry file measurements

Tag	Description	Value [m]
a	Waveguide width	0.08636
d	Waveguide length	0.075
xc	Waveguide position	-
l_x	Box side length	0.60
l_y	Box depth	0.21
l_w	Wood thickness	0.02
h	Sand level start	0.035
s	PMA/PML thickness	0.055
xi	Target x-centre	-
yi	Target y-centre	-
ai	Target radius	-

The value of parameter s has been artificially set and values of xc, xi, yi and ai depend on the antenna position and on the specific target used. Moreover, target boundaries are predefined as plastic but depend also on the concrete experiment.

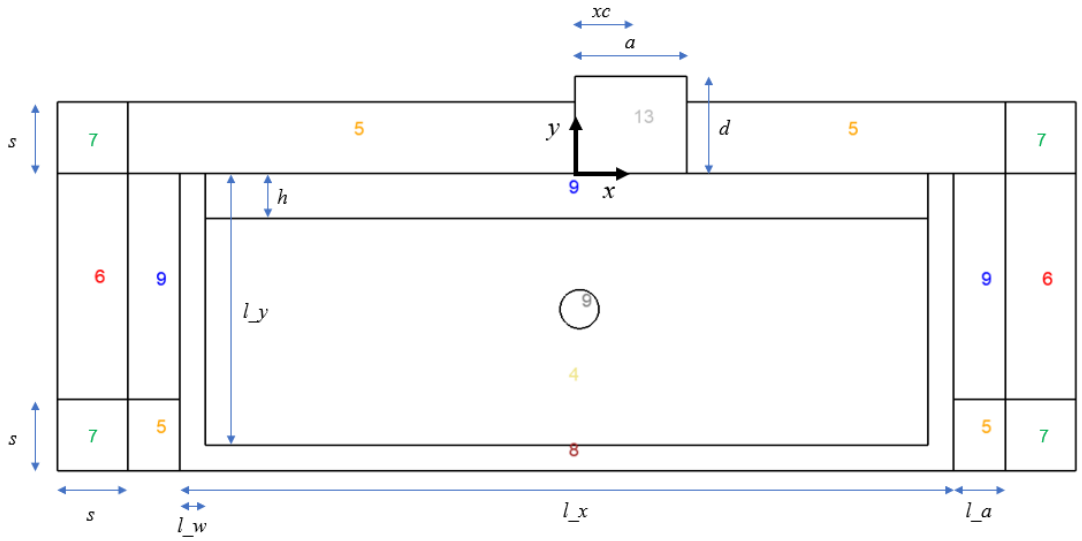

Figure 2.9 Geometry of simulations

2.2.2.2 Physical parameters

In order to describe the physical behavior of the various materials, different parameters are set and introduced to the numerical solver. The values of these parameters are presented in Table 2.3.

Table 2.3 Phyisical parameters

Description	Value
Waveguide ε_r	2.3884
Waveguide conductivity	0.001
Modes permitted in the waveguide	1
PMA/PML ε_r	1
PMA/PML conductivity	0
PMA reflection coefficient	0.0001
PMA order	2
Sand ε_r	2.3884
Sand conductivity	0.001
Air ε_r	1
Air conductivity	0
Wood ε_r	3
Wood conductivity	0.0005

Relative dielectric permittivity of sand has been calculated extracting from the waveguide antenna datasheets its cut-off frequency, which is 1.74 GHz. Then, as it is filled with dry sand, its cut-off frequency decreases with the following equation:

$$f_{c,sand} = \frac{f_{c,0}}{\sqrt{\varepsilon_{sand}}} \tag{2.9}$$

Where ε_{sand} is the sand relative dielectric permittivity.

In order to find the exact value of ε_{sand} after having filled the waveguide, we measure $S_{11}(\omega)$ experimentally at first laboratory position and look for the cut-off frequency at the VNA display. In this case, we have found $f_{c,sand} = 1.11\ GHz$ as can be seen in Figure 2.10:

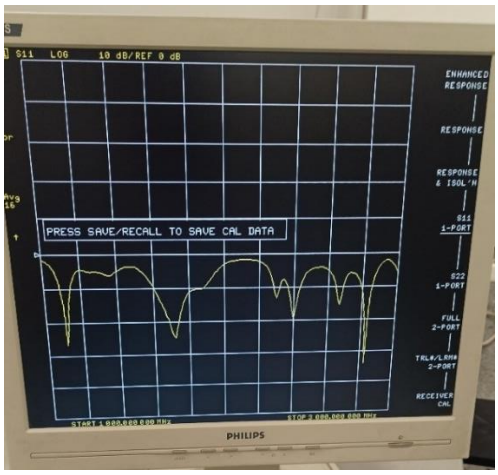

Figure 2.10 Reflection coefficient of the adopted antenna filled with sand measured at first laboratory position in front of the sand box without target

Then, by (2.9), a value of $\varepsilon_{sand} = 2.3884$ is obtained and is used to model dry sand inside the waveguide and the wood box in simulations.

2.2.2.3 Frequencies and positions used

The starting frequency has been chosen by using approximately a 30% margin above the cutoff frequency found in last section, therefore a value of 1.45 GHz is used. Regarding the stopping frequency, the VNA is configured up to 3 GHz, but in simulations and consequently when obtaining results only frequencies up to 2 GHz are selected. The frequency step is always 10 MHz. These frequency range is the one used also for experimental measures.

Regarding the positions in which measurements are taken, which are given by parameter xc, they depend on the specific data acquisition that is been carried out. Nevertheless, there is a difference between the coordinate origin used in simulations, located in the center of the configuration, and in the laboratory, placed at the right part of the wood box, that must be considered. This is represented in Figure 2.11.

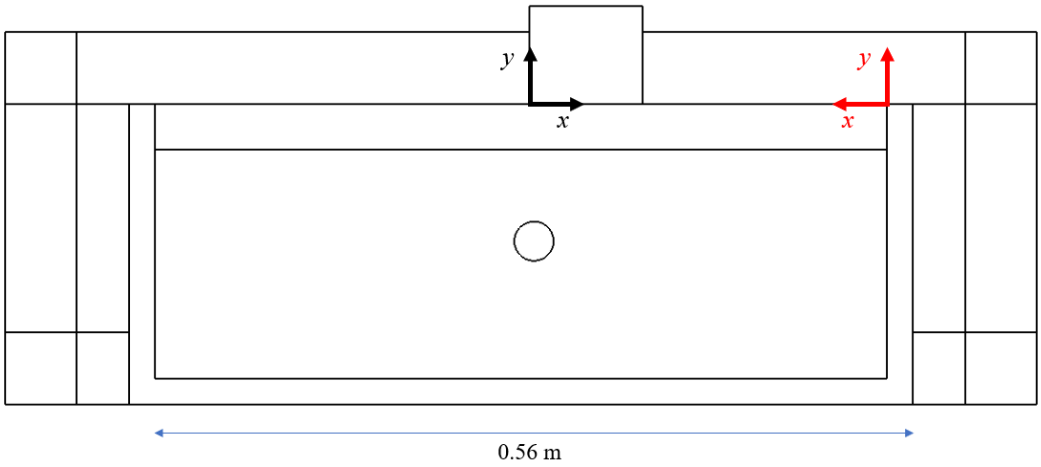

Figure 2.11 Coordinate Origins. In black: Simulations. In red: Laboratory.

Therefore, a mapping process from x-coordinates of laboratory positions to x-coordinates of simulation positions must be performed in order to perform simulations accurately. Moreover, in the laboratory the measures are taken from right to left, while in the simulations these are listed from left to right. Thus, the number that identifies each measurement is the inverse of the other case.

2.2.2.4 Simulation outputs

When a simulation is performed, first of all GMSH generates a mesh file describing the geometry of the problem for each antenna position. This files, along with the physical properties of materials, are introduced to the numerical solver and both the *.s1p files for each position at all frequencies and a *.msh file describing the E_z field component for each position and frequency are created.

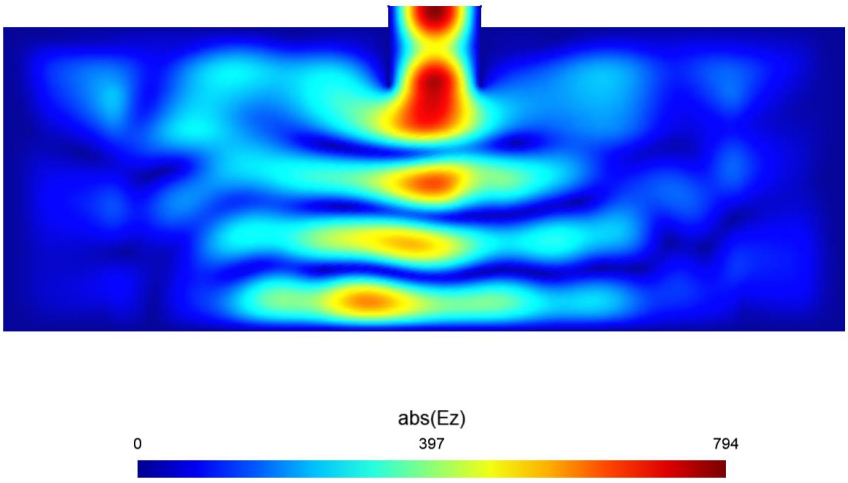

Figure 2.12 Magnitude of z-component of electric field in the simulation with a buried plastic target at antenna position number 17 and frequency 1.77 GHz

Afterwards, a bash script is run in order to merge in one *.s1p file for each of the positions all values of the different frequencies in that position.

Chapter 3
Results

In this chapter, the different experiments carried out are presented. In particular, different tests were conducted in three days using various calibration targets and test target positions. In the aim of obtaining more understandable results, measures obtained in frequency domain ($S_{11}(\omega)$) in several positions are displayed in time domain as B-Scans after applying the discrete fast Fourier transform. In these representations, a value of the amplitude of the received wave is presented for a certain time (y-axis) and a certain position (x-axis).

Regarding the time axis, it can be related to the distance at which the reflection has occurred, which in this case is the depth in the sandbox. Therefore, taking c_{sand} as the propagation speed in sand:

$$c_{sand} = \frac{c}{\sqrt{\varepsilon_{sand}}} = 1.94 * 10^8\ m/s \tag{3.1}$$

The mentioned relation is the following:

$$t_0 = 2 * \frac{d}{c_{sand}} \tag{3.2}$$

Results are presented for both calibration methods exposed in 2.1.1 and 2.1.2. However, as the necessary freespace measures of the antenna for 2.1.2 method were acquired in the second experimental session, this second method results are only reported for measures of this precise day.

As a summary of all experiments conducted, Table 3.1 is presented, where the characteristics of the three sessions in which measures have been taken are detailed. These include the calibration target used and the number of positions in which calibration data has been acquired, the test target buried and its location and the references to the figures in which results of both calibration methods are shown.

Table 3.1 Summary of experiments

Session		First	Second		Third	
Calibration target		Sand without target	Sand without target	Metal plate	Sand without target	Metal pipe
Number of calibration positions		8	8	8	7	7
Test target		Void plastic pipe				
Test target position		$y = -0.081\ m$	$y = -0.081\ m$		$y = -0.101\ m$	
		$x\ (lab) = 0.185\ m$	$x\ (lab) = 0.185\ m$		$x\ (lab) = 0.230\ m$	
		$x\ (sim) = 0.095\ m$	$x\ (sim) = 0.095\ m$		$x\ (sim) = 0.050\ m$	
Results	First method	Figure 3.7	Figure 3.13	Figure 3.15	Figure 3.22	Figure 3.23
	Second method	-	Figure 3.14	Figure 3.16	-	-

3.1 First measurement session

3.1.1 Calibration target

This data is specifically used to obtain the antenna's transfer functions with the method specified in 2.1.1, therefore (2.3) can be applied to obtain the calibrated coefficients. In this case, these measures were taken in front of the sand box without any target buried in it.

Figure 3.1 Scenario of first session calibration measurements

Moreover, eight antenna positions (*xc* parameter in
Table 2.2) were used along with the range of frequencies between 1.45 GHz – 2 GHz each 10 MHz. The concrete values for both laboratory and simulations axes are shown in Table 3.2.

Table 3.2 Antenna center positions of first session calibration measurements

Number	0	1	2	3	4	5	6	7
Laboratory [m]	0.11	0.16	0.21	0.26	0.31	0.36	0.41	0.46
Simulations [m]	- 0.18	- 0.13	- 0.08	- 0.03	0.02	0.07	0.12	0.17

Then, simulations are performed following section 2.2.2. In order to replicate the experimental configuration, GMSH file is defined without any target inside the sand and the positions of Table 3.2 are introduced. The corresponing results, expressed in the temporal domain as B-Scans, are presented in Figure 3.2.

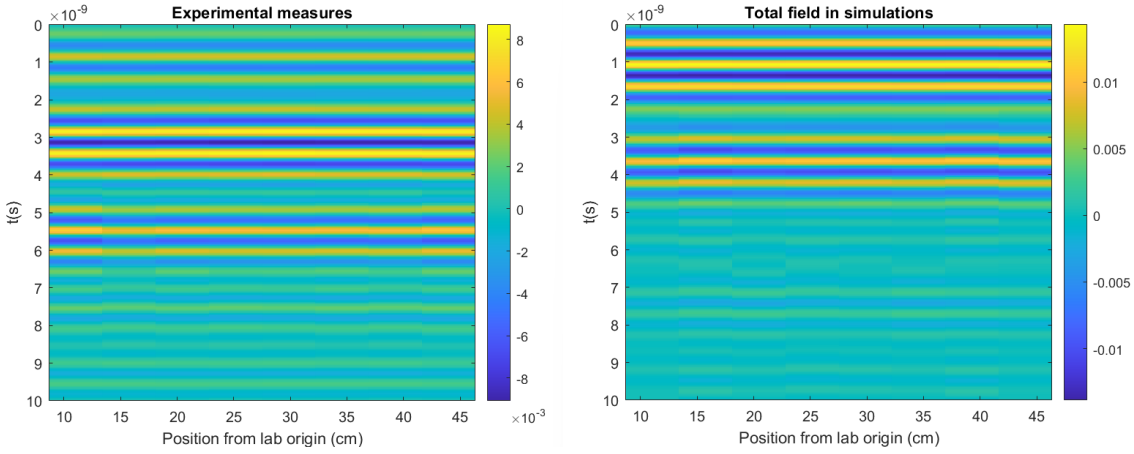

Figure 3.2 Experimental and simulated B-Scans of first session calibration measurements

At this point, following the procedure described in section 2.1.1, the corresponding antenna transfer functions are obtained (Figure 3.3) and will be applied to calibrate measurements by equation (2.3).

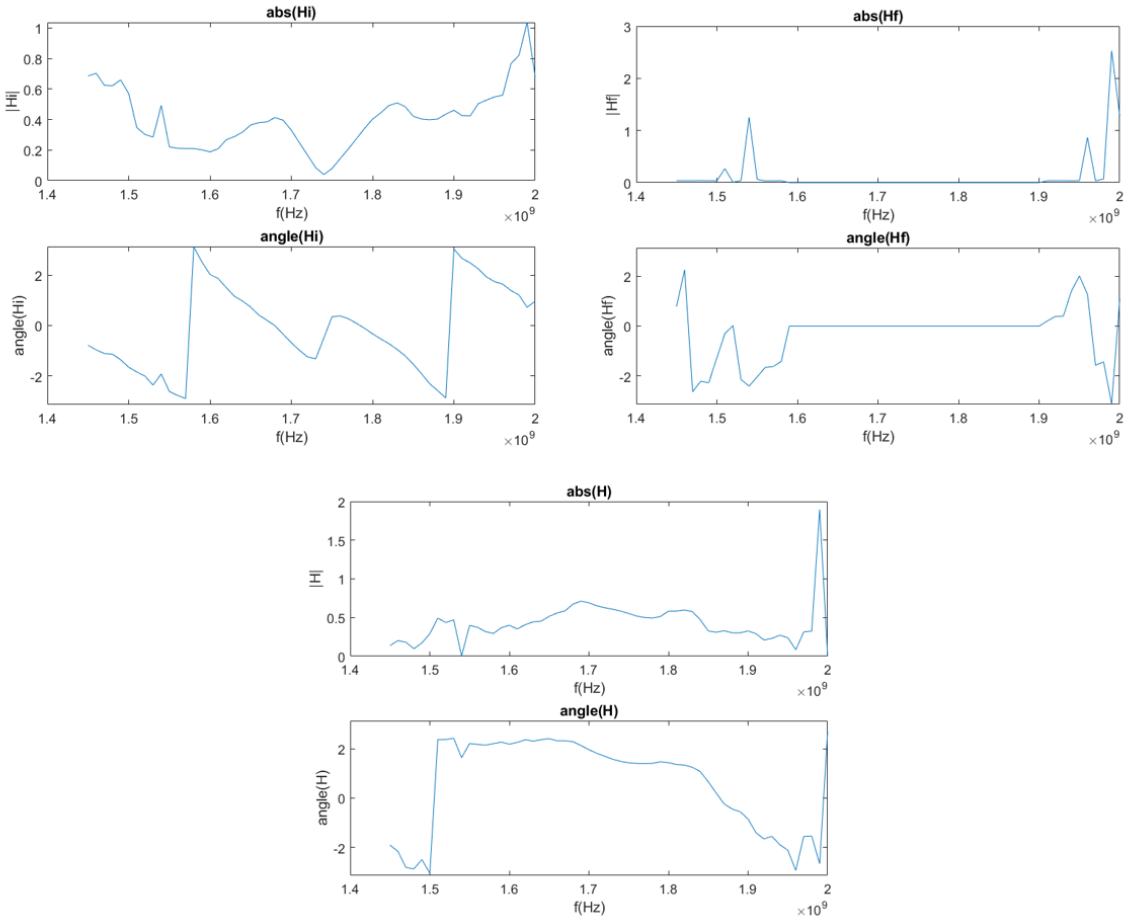

Figure 3.3 Transfer functions obtained for first session calibration measurements and first calibration method

3.1.2 Test target

These measurements are obtained with the purpose of testing the different calibration methods (2.1.1, 2.1.2). In particular, the target used consists of a void plastic pipe of radius 2.1 cm.

Figure 3.4 Plastic target

In this case, the target position is detailed in Table 3.3.

Table 3.3 Test target location in first session set of measurements

Coordinate	Value [m]
y_i	- 0.081
x_i (laboratory)	0.185
x_i (simulations)	0.095

Moreover, $Q = 34$ antenna positions each 1 cm are used to take measurements of S_{11} coefficients, which are reported in Table 3.4.

Table 3.4 Measurement positions in first session set

Number	0	1	2	…	31	32	33
Laboratory [m]	0.11	0.12	0.13	…	0.42	0.43	0.44
Simulations [m]	- 0.16	- 0.15	- 0.14	…	0.15	0.16	0.17

3.1.3 Results

3.1.3.1 Simulations

Initially, simulations are performed to replicate the experimental scenario following the procedure explained in Section 2.2.2. Consequently, the plastic target is defined at its location in GMSH file and the 34 measurement positions of Table 3.4 are simulated in the range of 1.45 GHz – 3 GHz each 10 MHz. The results of the total and the scattered field, expressed as B-Scans are shown in Figure 3.5.

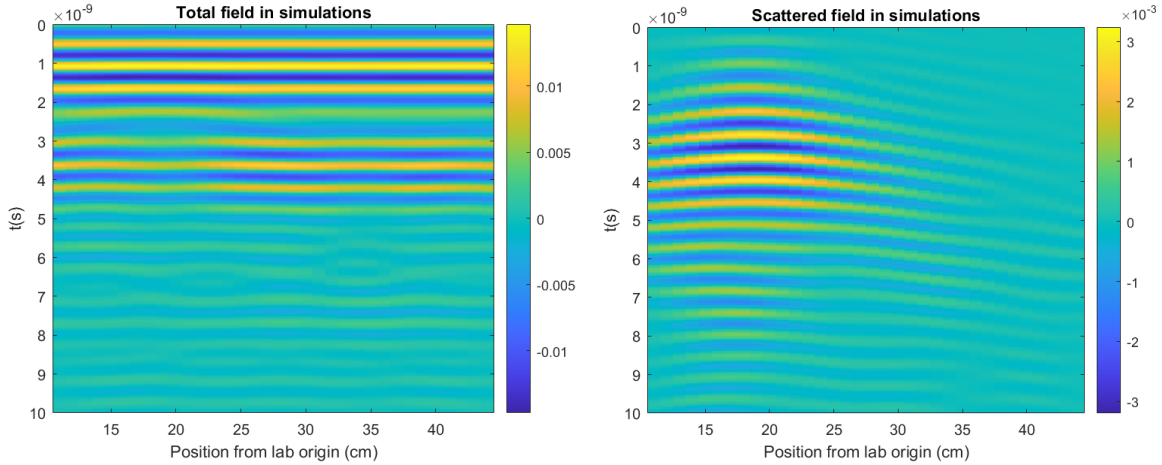

Figure 3.5 Simulations of first session measurements

In the total field B-Scan, multiple reflections between the antenna and the surface are observed, as well as the reflections due to the existence of the metal plate (PEC surface in simulations) placed under the wood box. Meanwhile, in the scattered field B-Scan, only the reflections caused by the target and the metal plate are visible.

3.1.3.2 Uncalibrated data

The results of laboratory measures taken according to Section 3.1.2, presented as the corresponding B-Scans of the total and scattered field are in Figure 3.6.

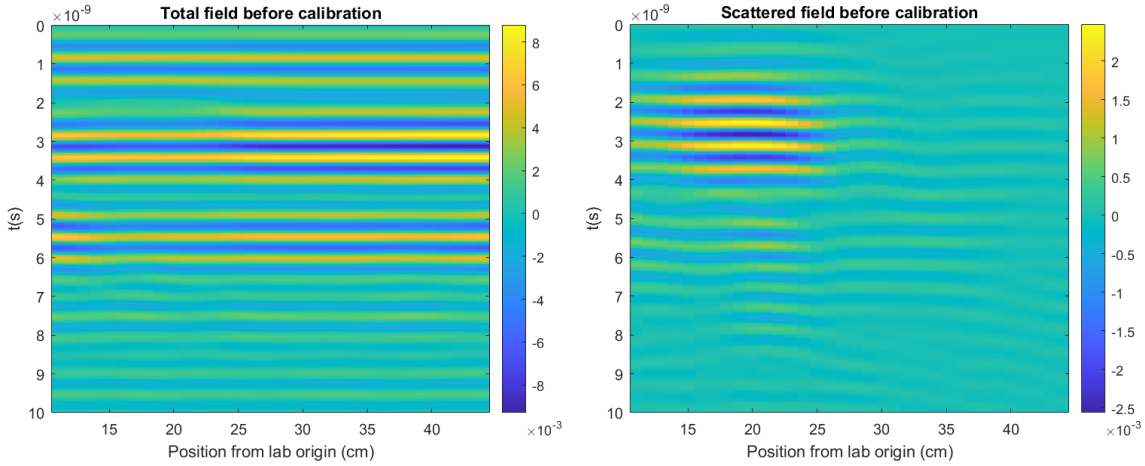

Figure 3.6 B-Scans of uncalibrated first session measurements

3.1.3.3 Calibrated data

In this case, the resultant transfer functions of the first calibration method presented in

Figure 3.3 are used to apply equation (2.3) to the uncalibrated coefficients through a MATLAB script. The obtained coefficients for each position, presented as B-Scans, can be seen in Figure 3.7.

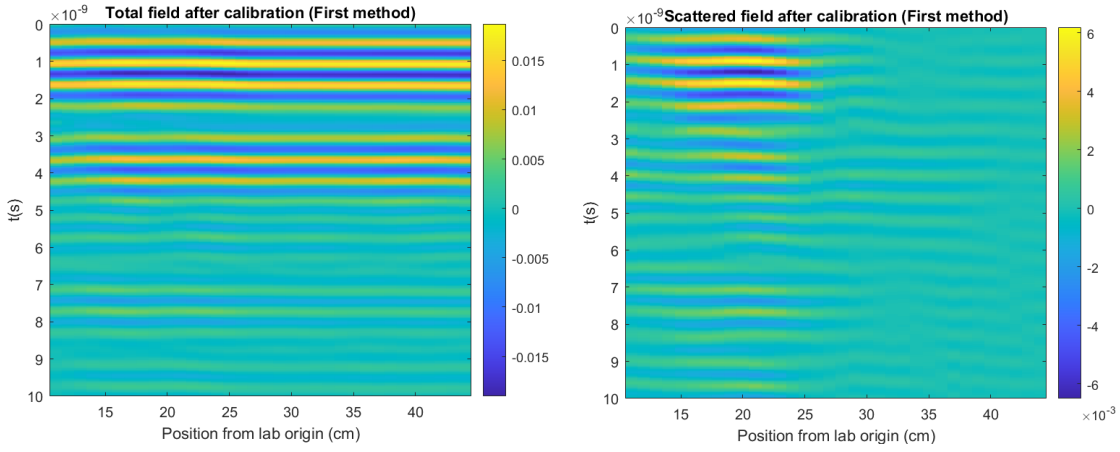

Figure 3.7 Calibrated data of first session with first method

3.2 Second measurement session

As have been explained before, the necessary measures of antenna in freespace to carry out the calibration method proposed in 2.1.2 were taken in this session. Therefore, this is the only case in which both calibration methods are used and thus evaluated.

3.2.1 Calibration target

The targets for calibration used in this session are two: first, as in the first one, measures in front of the sand box without any target buried inside it and second, measures in front of a metal plate.

3.2.1.1 Sand without target

In this case, the procedure followed is analogous to the one in 3.1.1. Therefore, the same positions and configuration are used.

3.2.1.2 Metal plate

The configuration proposed consists of locating a metal plate on the sand surface and obtain measurements in eight positions with the antenna in front of it. The distance between the antenna and the metal plate is assumed to be the same value *h* described in Table 2.2 Geometry file measurements.

Figure 3.8 Scenario for second session calibration measures with metal plate

Table 3.5 Antenna center positions of second session calibration measurements with metal plate

Number	0	1	2	3	4	5	6	7
Laboratory [m]	0.11	0.16	0.21	0.26	0.31	0.36	0.41	0.46
Simulations [m]	- 0.18	- 0.13	- 0.08	- 0.03	0.02	0.07	0.12	0.17

In the simulations, a PEC layer is defined on top of the sand in order to replicate the real scenario. Therefore, B-Scans of the experimental measures and simulations in the eight positions are obtained and represented in Figure 3.9.

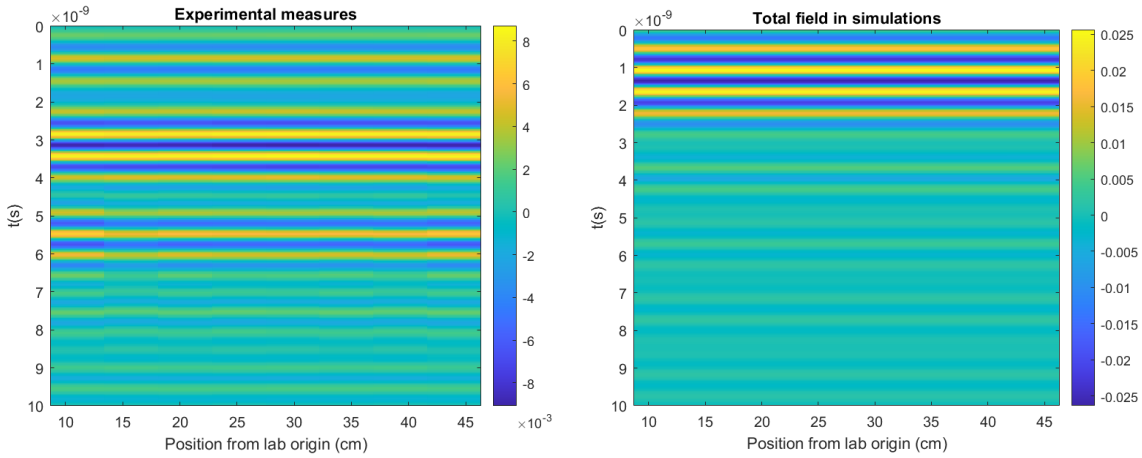

Figure 3.9 Experimental and simulated B-Scans of second session calibration measurements with metal plate

Following the procedures described in sections 2.1.1 and 2.1.2, the corresponding antenna transfer functions are obtained and can be observed in Figure 3.10 and Figure 3.11.

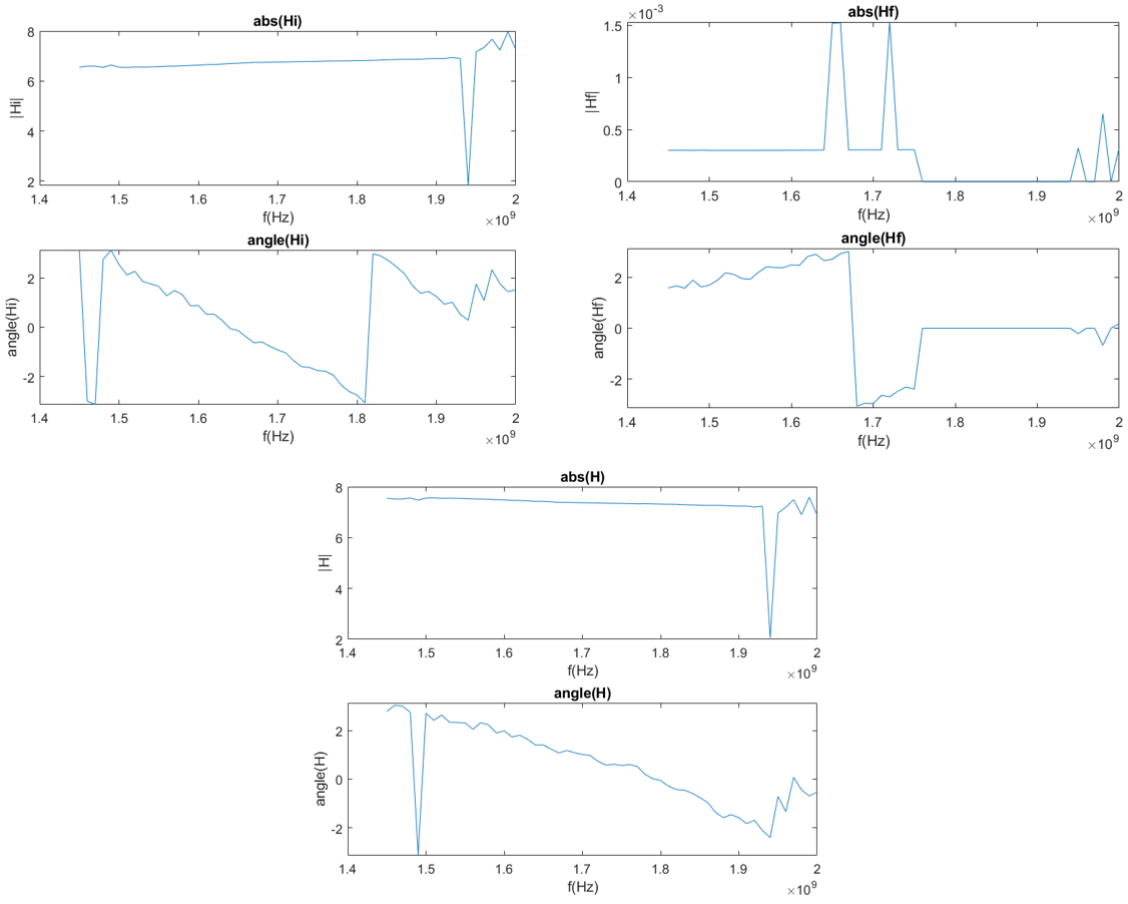

Figure 3.10 Transfer functions obtained for second session calibration measurements with metal plate and first calibration method

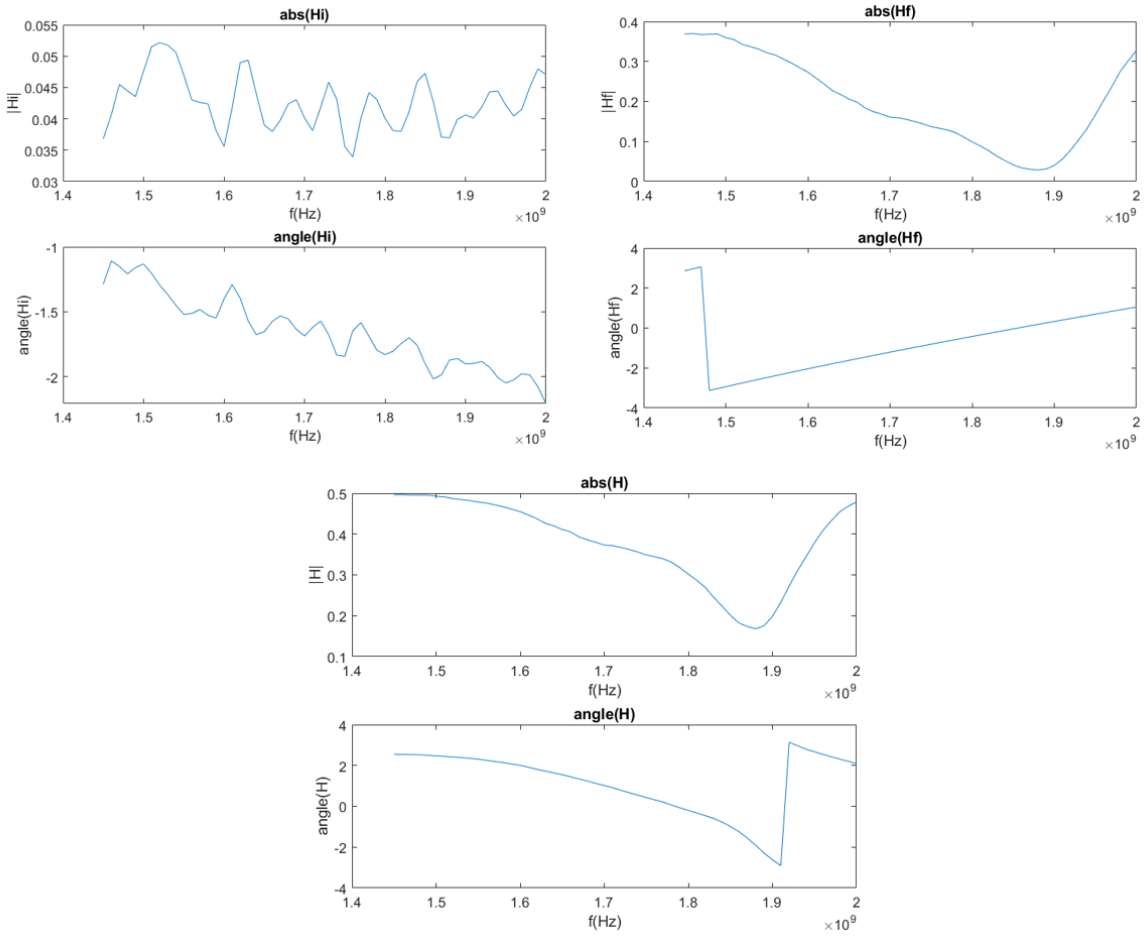

Figure 3.11 Transfer functions obtained for second session calibration measurements with metal plate and second calibration method

3.2.2 Test target

The target used in this case is the same void plastic pipe as in the measurements of the first session (Figure 3.4). Moreover, its location is the same as the described in Table 3.3 and the antenna positions in which data is acquired are the ones of Table 3.4.

3.2.3 Results

3.2.3.1 Simulations

As the test target configuration and the measurements positions have not changed, the simulations used as reference in this section are the ones carried out previously in Section 3.1.3.1.

3.2.3.2 Uncalibrated data

As in the previous case, the B-Scans of the total and the scattered field of experimental measures before the calibration process are presented in Figure 3.12.

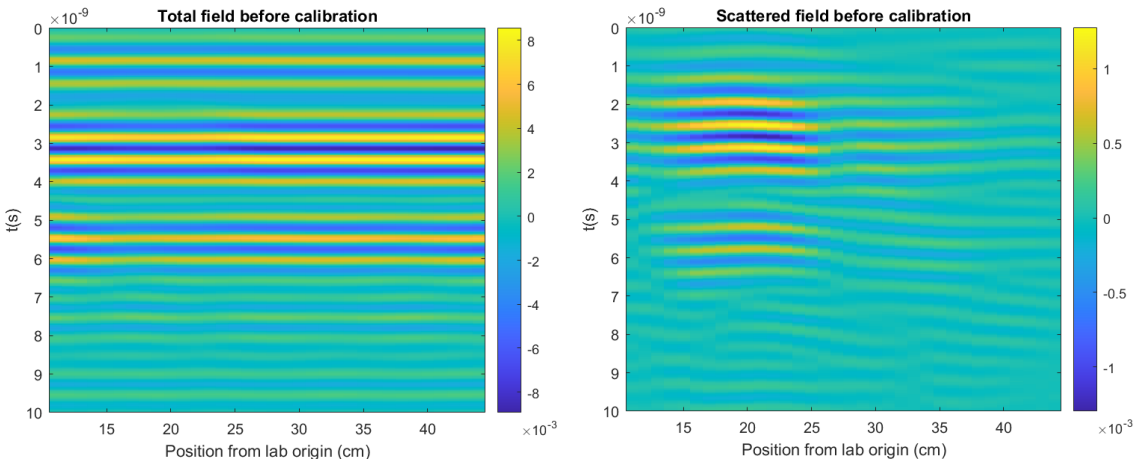

Figure 3.12 B-Scans of uncalibrated second session set of measurements

3.2.3.3 Calibrated data

First of all, calibrated measures using the first calibration target (3.2.1.1) and both transfer functions of calibration methods 2.1.1 and 2.1.2 are shown in Figure 3.13 and Figure 3.14.

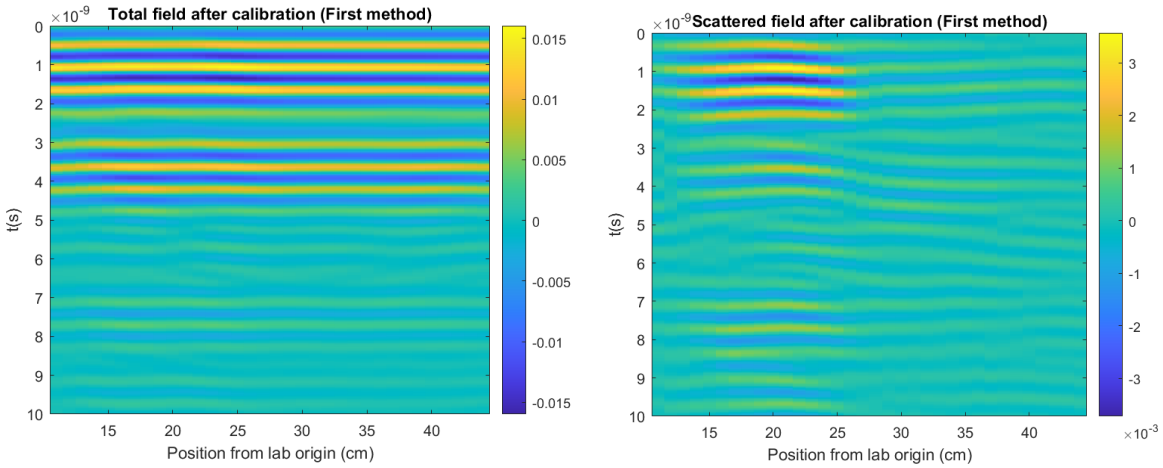

Figure 3.13 Calibrated data of second session with first calibration target and first method

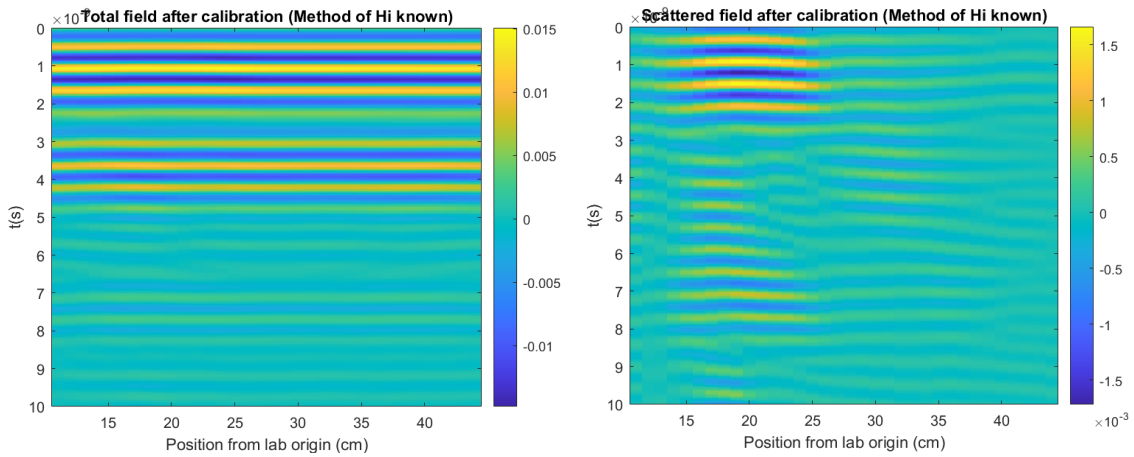

Figure 3.14 Calibrated data of second session with first calibration target and second method

The results obtained using as calibration data the measures with the metal plate (3.2.1.2) and both calibration methods (2.1.1 and 2.1.2) are presented in Figure 3.15 and Figure 3.16.

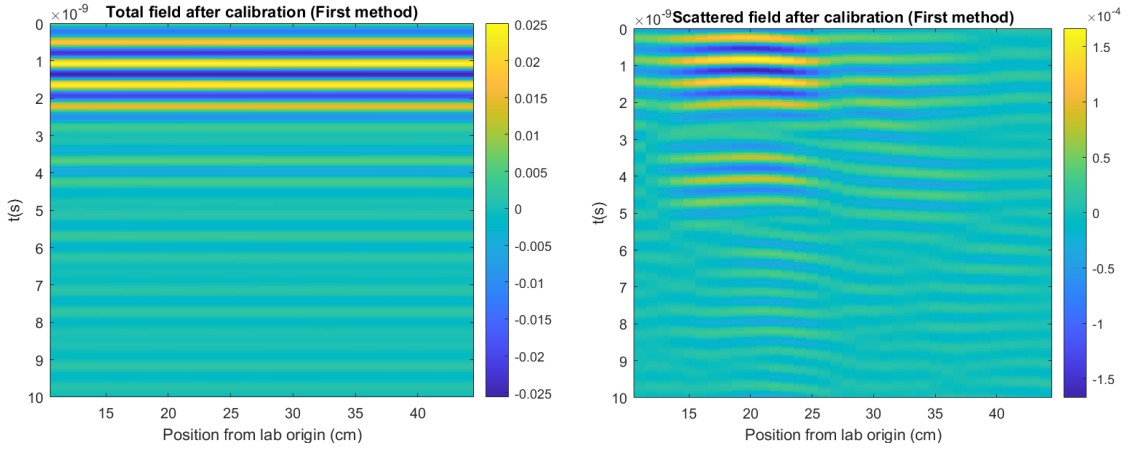

Figure 3.15 Calibrated data of second session with metal plate as calibration target and first method

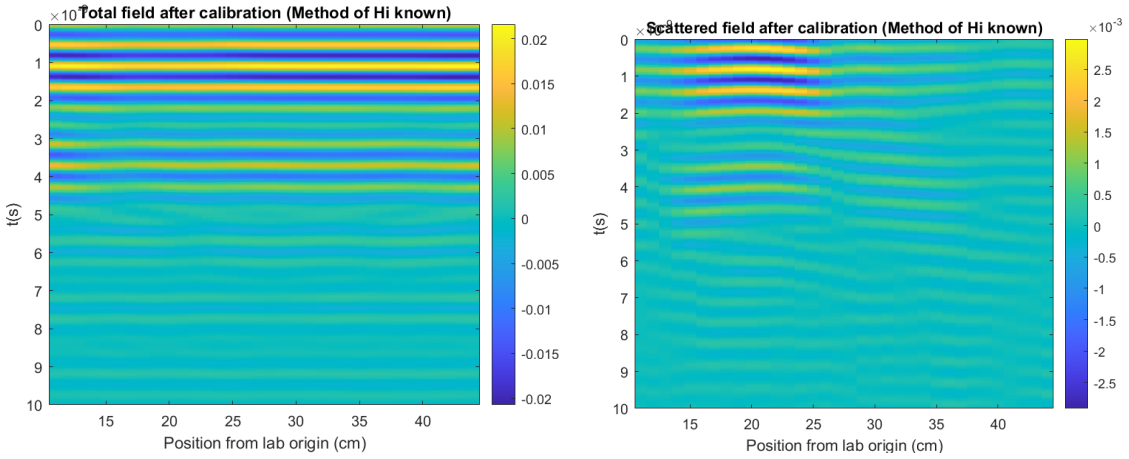

Figure 3.16 Calibrated data of second session with metal plate as calibration target and second method

3.3 Third measurement session

3.3.1 Calibration target

In this case, the two scenarios are the one with sand without target and with a buried metallic pipe.

3.3.1.1 Sand without target

The procedure followed is analogous as the one in Section 3.1.1, with the difference that in this case only the seven measurement positions detailed in Table 3.6 have been used.

Table 3.6 Antenna center positions of third session calibration measurements

Number	0	1	2	3	4	5	6
Laboratory [m]	0.11	0.16	0.21	0.26	0.31	0.36	0.41
Simulations [m]	- 0.18	- 0.13	- 0.08	- 0.03	0.02	0.07	0.12

3.3.1.2 Void metal pipe

In this case, a metallic tube with a radius of 1.5 cm is buried and data is obtained in seven positions along the measurement line. The location of the target is presented in Table 3.7 and the mentioned measurement positions in Table 3.8.

Figure 3.17 Metallic target

Table 3.7 Metallic target location

Coordinate	Value [m]
y_i	- 0.105
x_i (laboratory)	0.260
x_i (simulations)	0.020

Table 3.8 Antenna center positions of third session calibration measurements with metallic target

Number	0	1	2	3	4	5	6
Laboratory [m]	0.11	0.16	0.21	0.26	0.31	0.36	0.41
Simulations [m]	- 0.13	- 0.08	- 0.03	0.02	0.07	0.12	0.17

In simulations, the target radius is set to the new value and the target surface is defined as a PEC. Then, the B-Scans of Figure 3.18 are obtained.

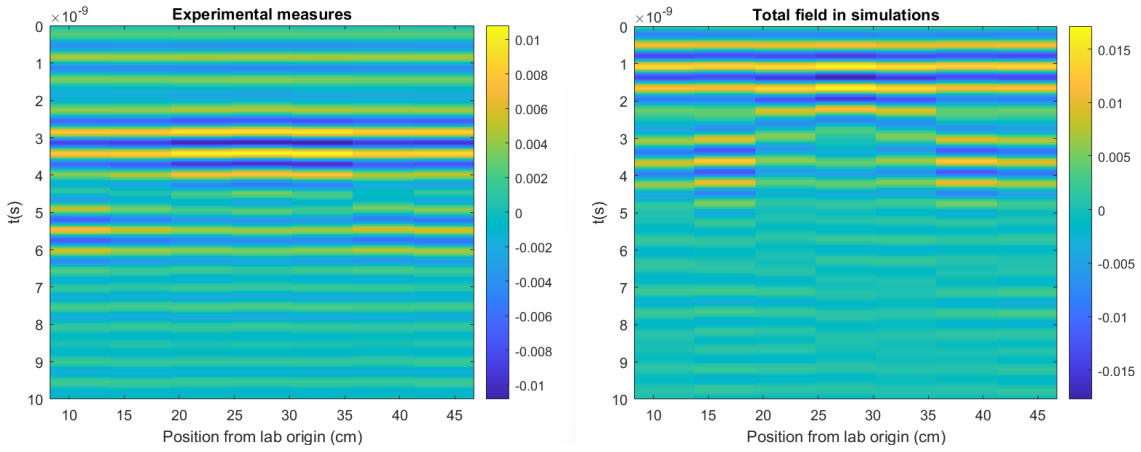

Figure 3.18 Experimental and simulated B-Scans of third session calibration measurements with metallic target

By the procedures described in sections 2.1.1 and 2.1.2, the corresponding antenna transfer functions are obtained and shown in Figure 3.19.

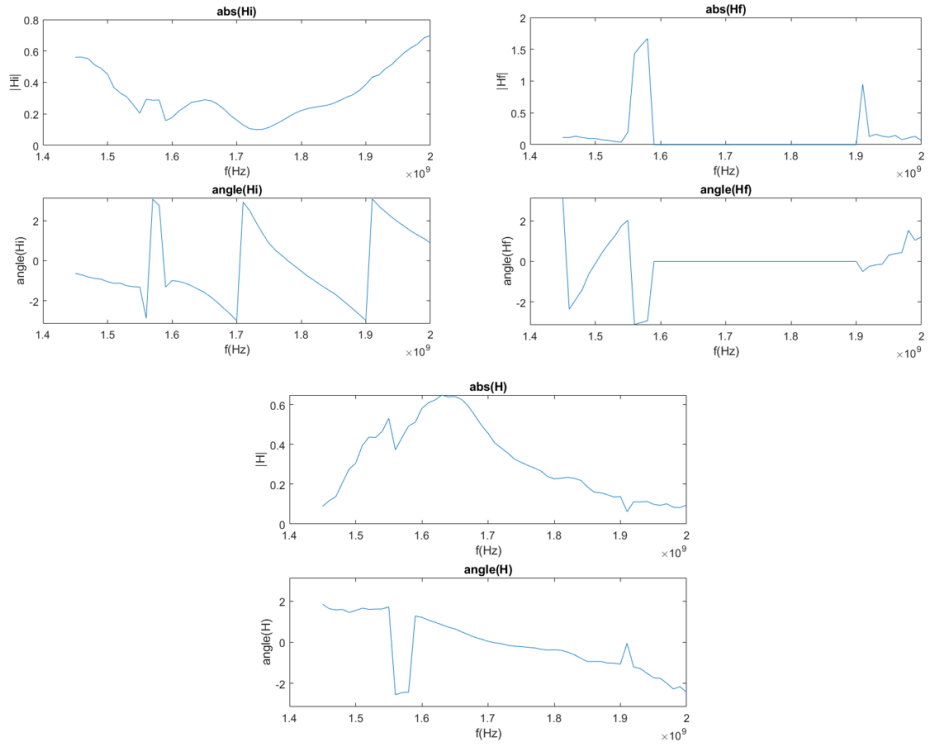

Figure 3.19 Transfer functions obtained for third session calibration measurements with metallic target and first calibration method

3.3.2 Test target

The test target employed is the same void plastic tube used in the rest of measurement days (Figure 3.4). Nevertheless, in this case its location has changed, the object has been buried in a deeper and more centered position with respect to the wood box, as can be observed in Table 3.9.

Table 3.9 Target location in third session set

Coordinate	Value [m]
y_i	- 0.101
x_i (laboratory)	0.230
x_i (simulations)	0.050

However, measurement positions are the same as in the first and second set and are detailed in Table 3.10.

Table 3.10 Measurement positions in thir session set

Number	0	1	2	…	31	32	33
Laboratory [m]	0.11	0.12	0.13	…	0.42	0.43	0.44
Simulations [m]	- 0.16	- 0.15	- 0.14	…	0.15	0.16	0.17

3.3.3 Results

3.3.3.1 Simulations

In this case, simulations are performed according to the modified target location and the measurement positions. Therefore, the B-Scans of the corresponding total and scattered fields can be observed in Figure 3.20.

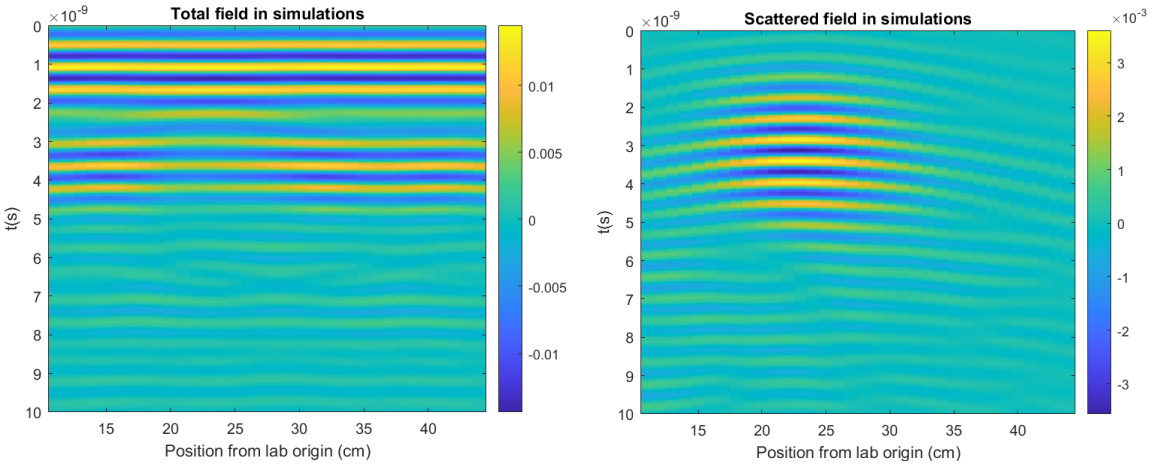

Figure 3.20 Simulations for third session set of measurements

3.3.3.2 Uncalibrated data

As with the other two cases, the resultant B-Scans of the total and scattered field of the experimentally obtained data before calibration are presented in Figure 3.21.

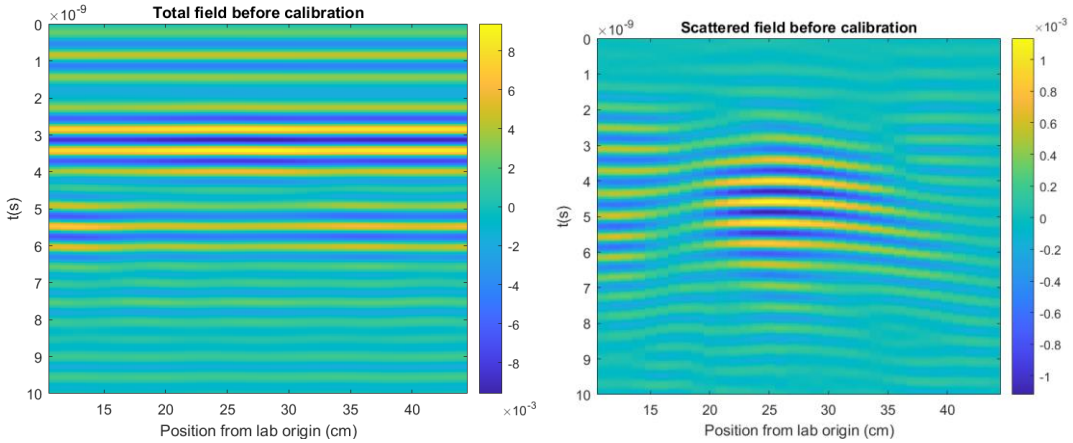

Figure 3.21 B-Scans of uncalibrated third session set of measurements

3.3.3.3 Calibrated data

In this case, results are presented for the two calibration targets employed (3.3.1.1 and 3.3.1.2) and the first calibration method (2.1.1) in Figure 3.22 and Figure 3.23.

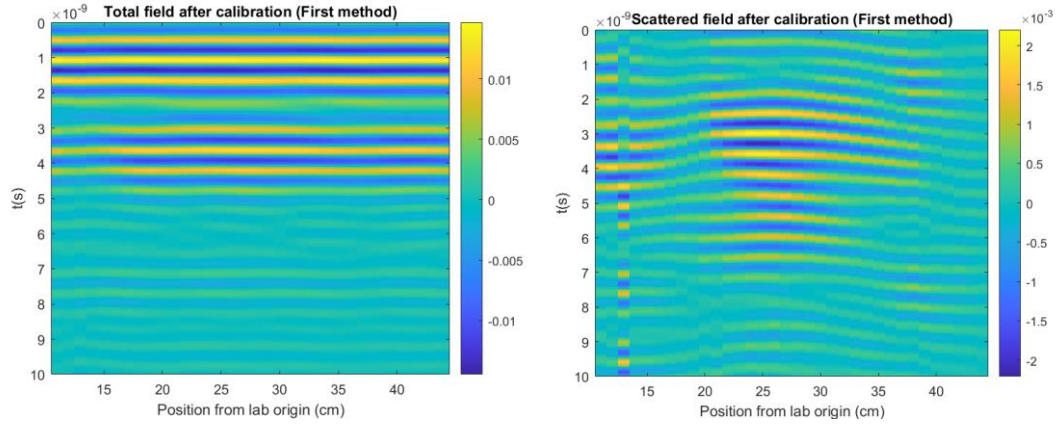

Figure 3.22 Calibrated data of third session with first calibration target and first calibration method

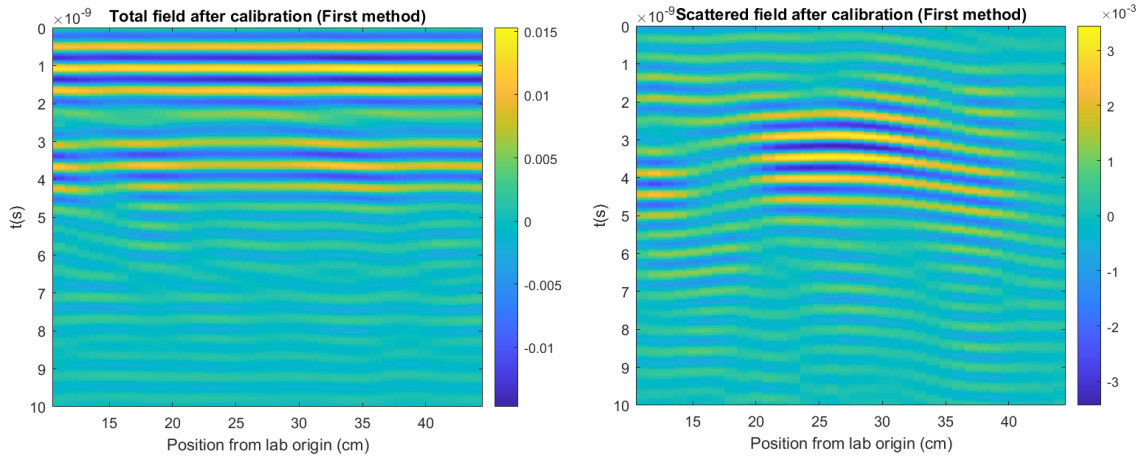

Figure 3.23 Calibrated data of third session with metallic pipe as calibration target and first calibration method

3.4 Comparison of results

In this chapter, a summary of the different calibration results is presented in order to facilitate the comparison between them and simulations. First, in Table 3.11 the index system used is presented and then, results can be observed. As the test target used is a void plastic pipe (Figure 3.4) in all cases, this information is not specified in Table 3.11.

Table 3.11 Index of results cases

Index	Case			Reference
	Session	Calibration target	Calibration method	
1	1st	Sand without target	1st	Figure 3.24
2	2nd	Sand without target	1st	Figure 3.25
3	2nd	Sand without target	2nd	Figure 3.26
4	2nd	Metal plate	1st	Figure 3.27
5	2nd	Metal plate	2nd	Figure 3.28
6	3rd	Sand without target	1st	Figure 3.29
7	3rd	Metallic pipe	1st	Figure 3.30

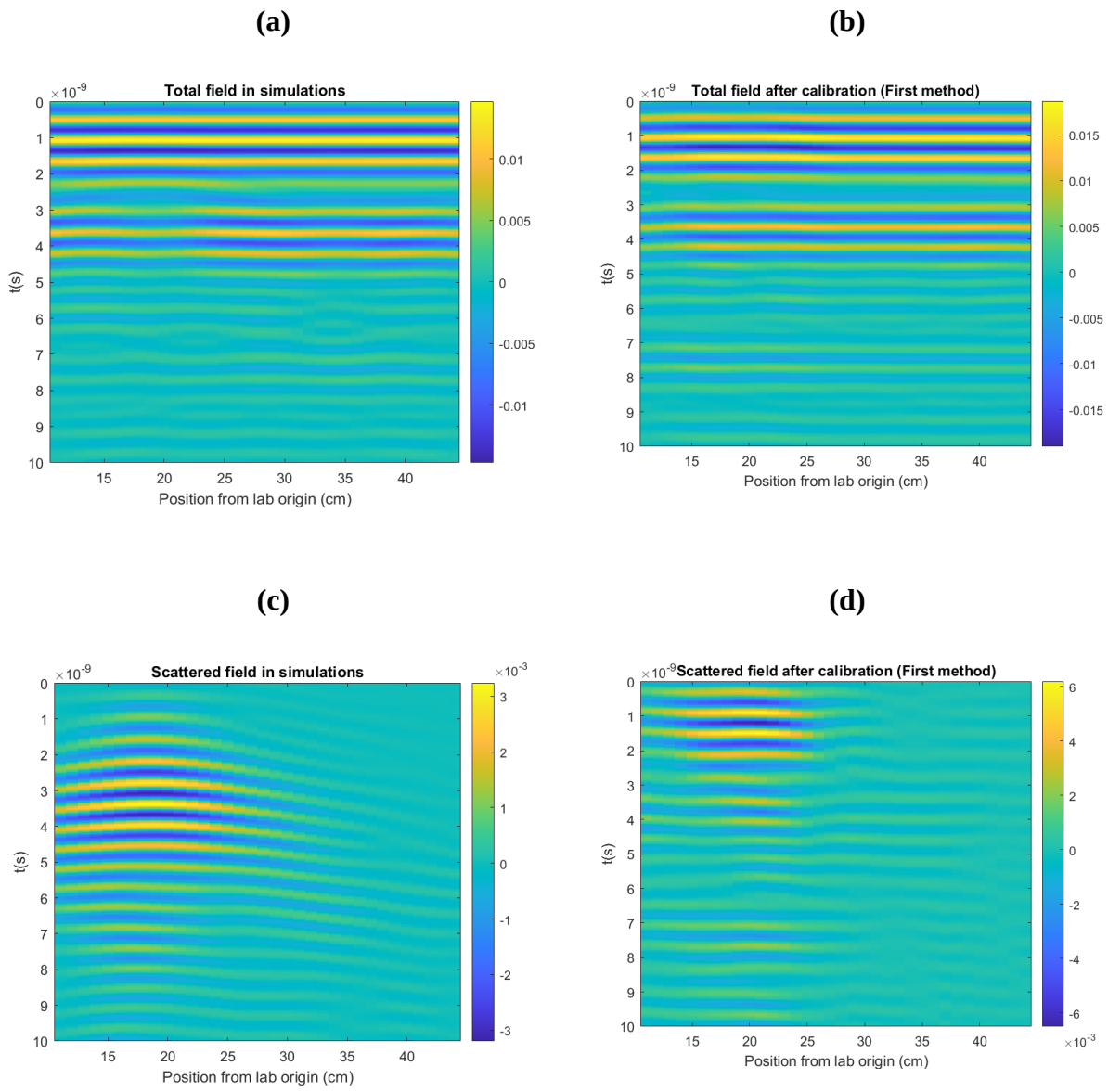

Figure 3.24 Results of case 1. (a) Simulted total field. (b) Calibrated total field. (c) Simulated scattered field. (d) Calibrated scattered field.

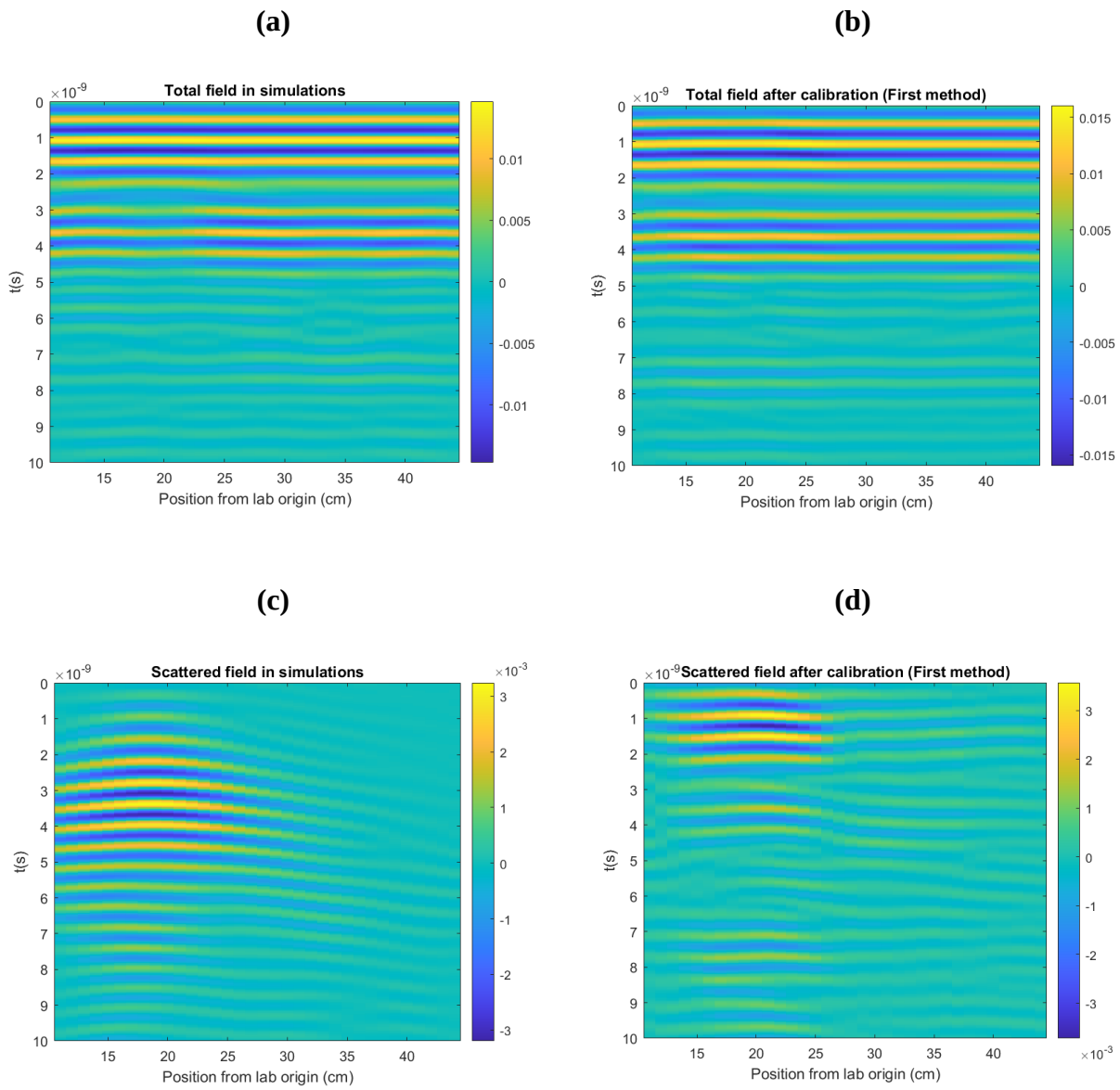

Figure 3.25 Results of case 2. (a) Simulted total field. (b) Calibrated total field. (c) Simulated scattered field. (d) Calibrated scattered field.

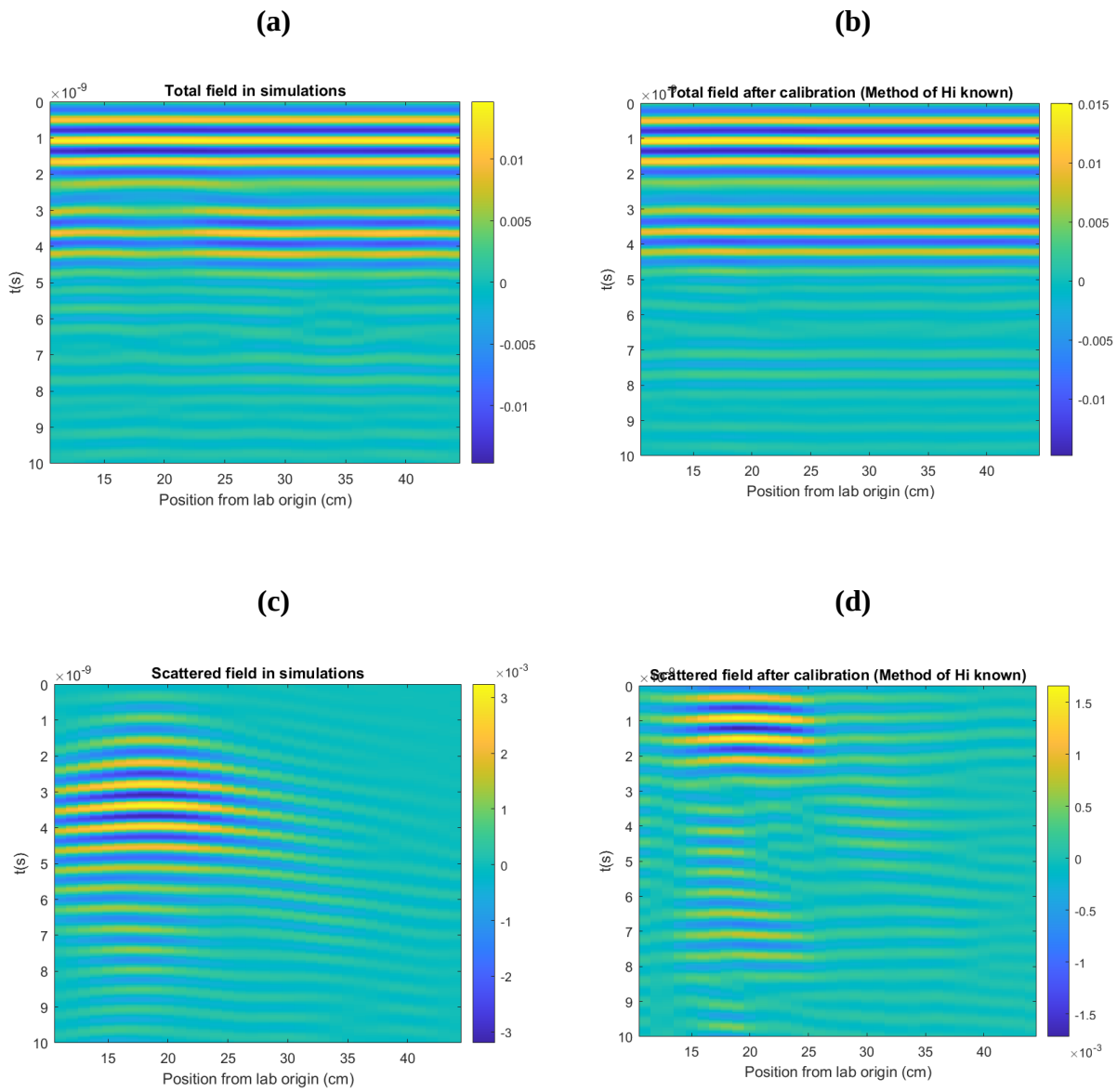

Figure 3.26 Results of case 3. (a) Simulted total field. (b) Calibrated total field. (c) Simulated scattered field. (d) Calibrated scattered field.

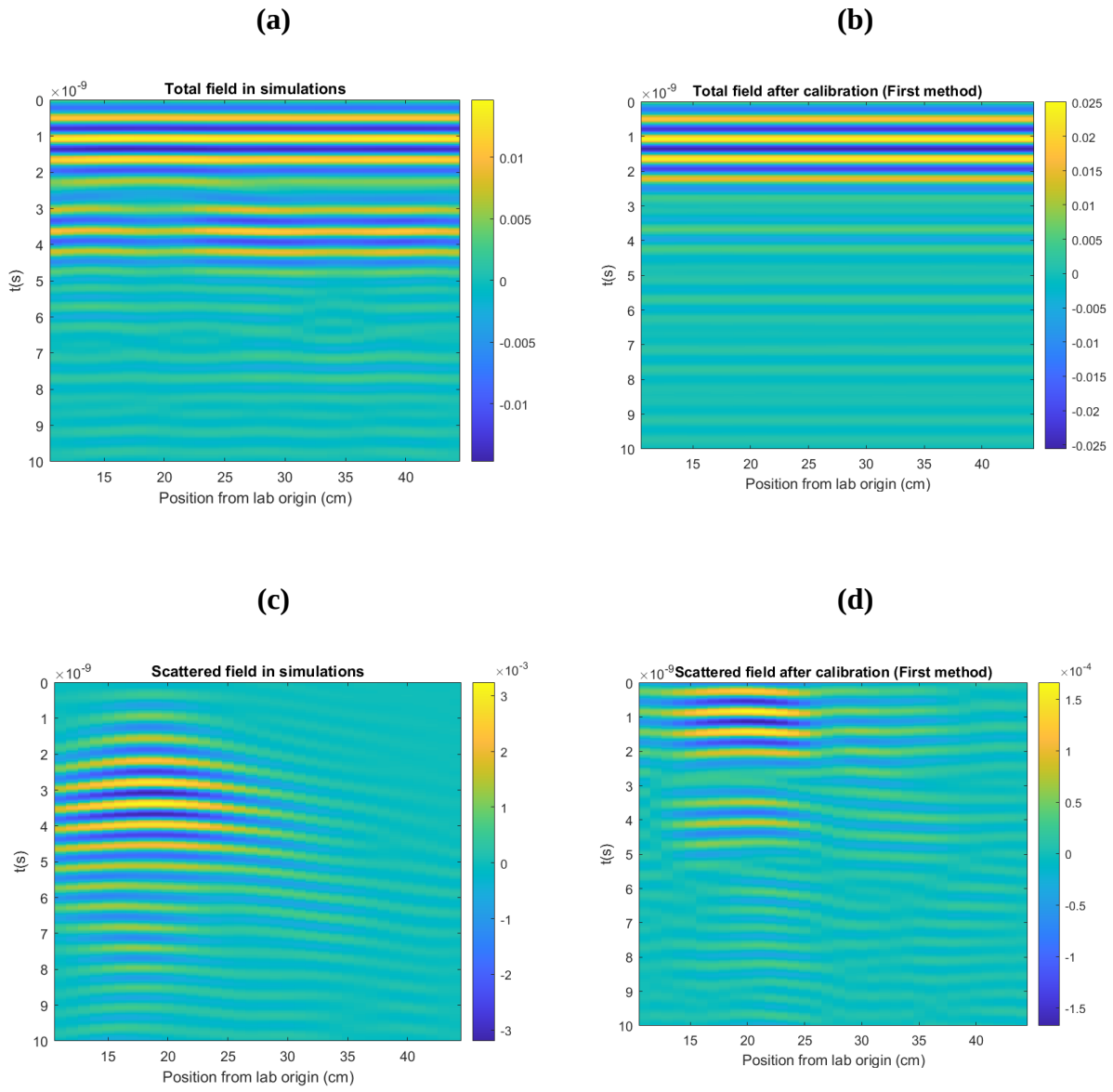

Figure 3.27 Results of case 4. (a) Simulted total field. (b) Calibrated total field. (c) Simulated scattered field. (d) Calibrated scattered field.

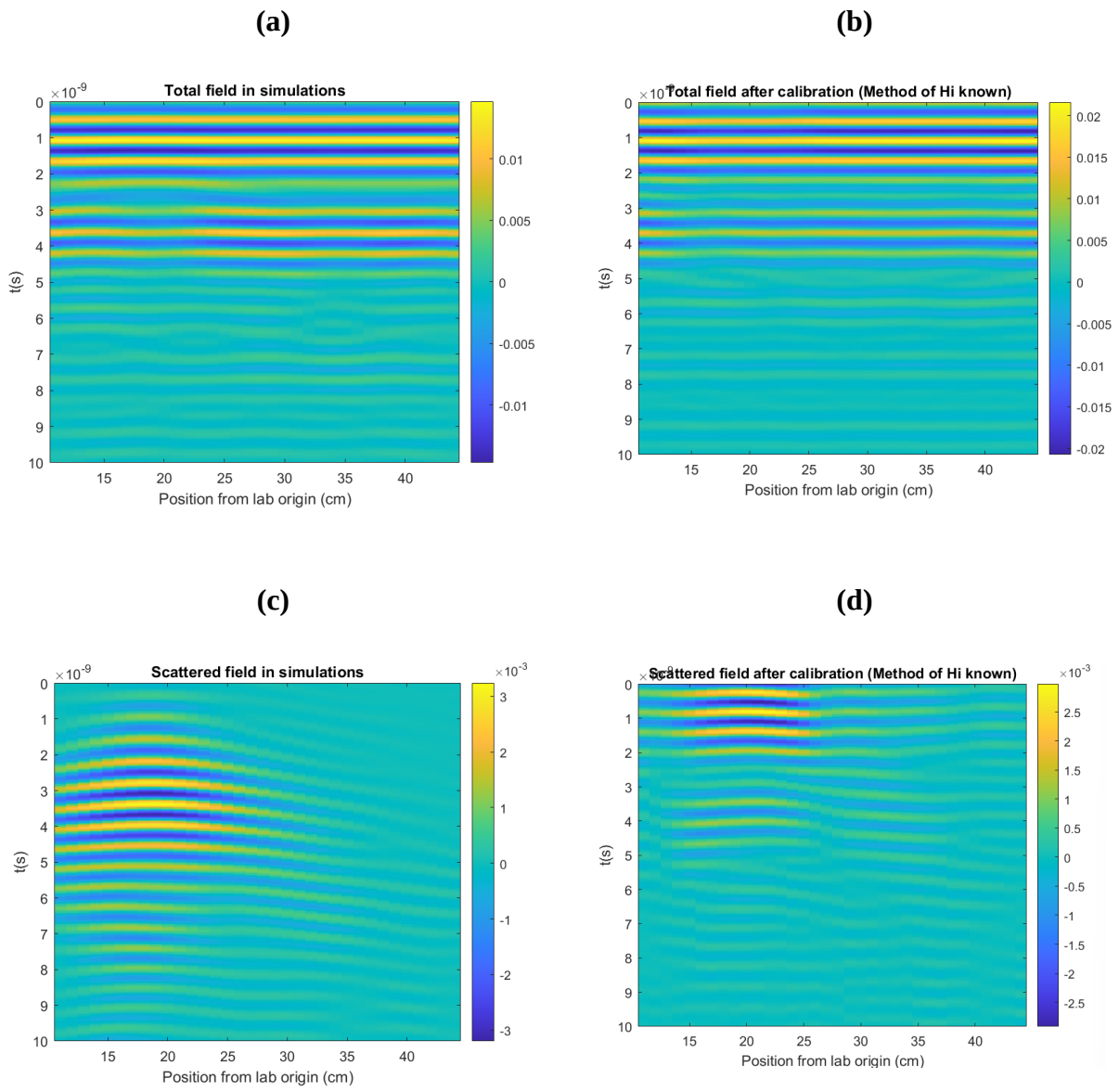

Figure 3.28 Results of case 5. (a) Simulted total field. (b) Calibrated total field. (c) Simulated scattered field. (d) Calibrated scattered field.

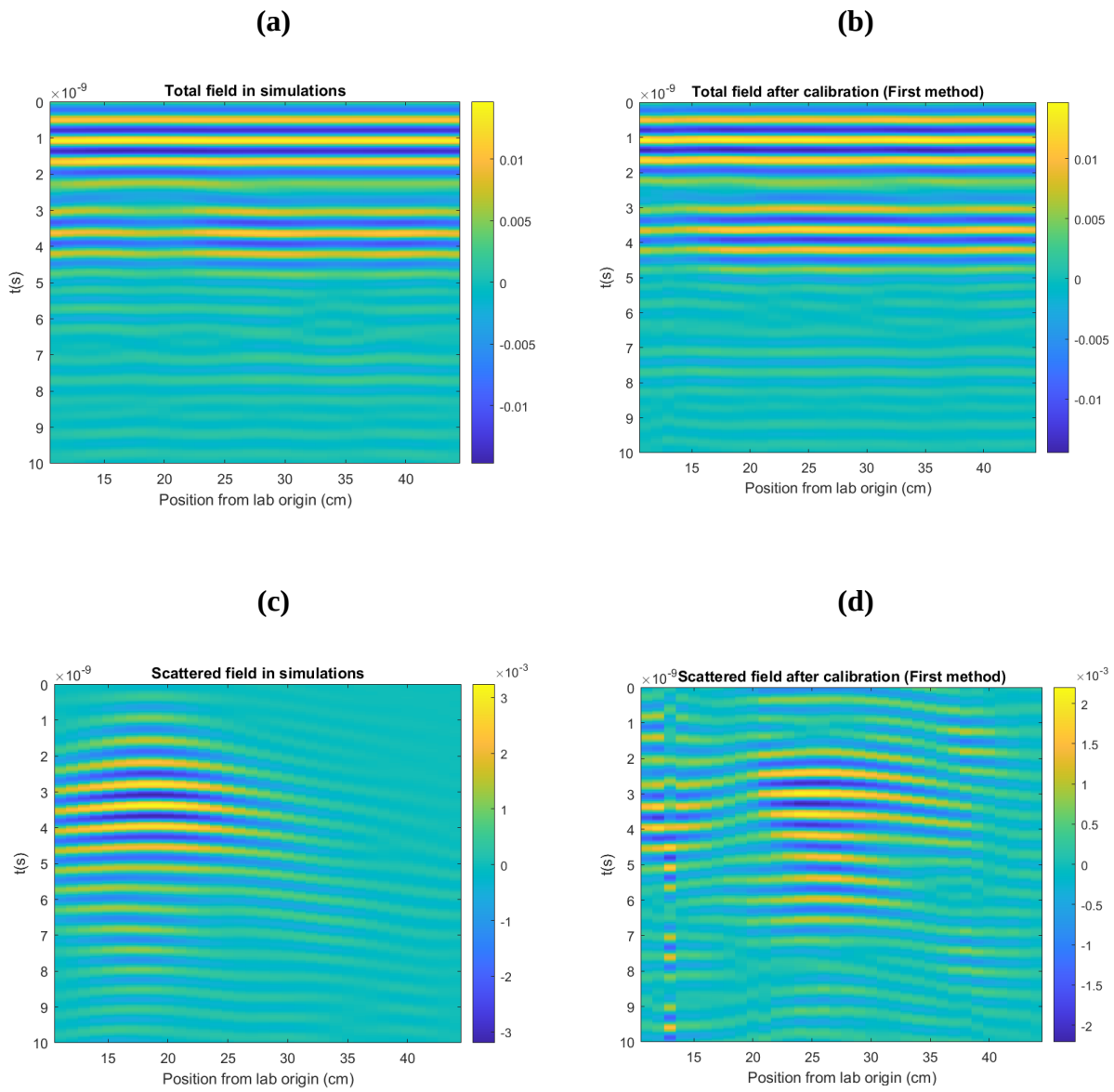

Figure 3.29 Results of case 6. (a) Simulted total field. (b) Calibrated total field. (c) Simulated scattered field. (d) Calibrated scattered field.

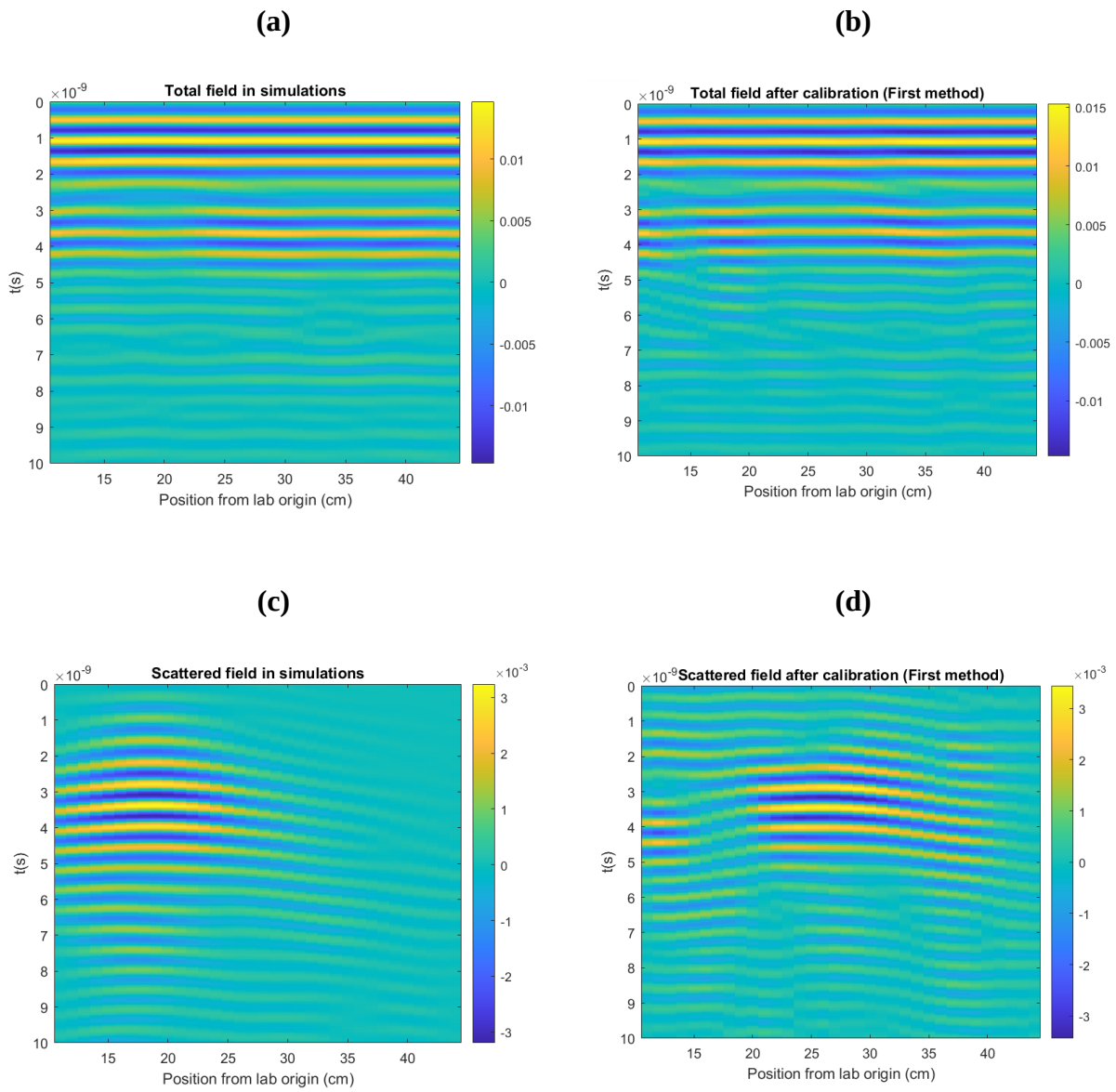

Figure 3.30 Results of case 7. (a) Simulted total field. (b) Calibrated total field. (c) Simulated scattered field. (d) Calibrated scattered field.

Chapter 4
Conclusions and future developments

In the present Thesis, various calibration methods for GPR S-parameters measurements have been evaluated. With this aim, the acquisition of experimental measures at the Applied Electromagnetics Laboratory of the Department of Electrical, Electronic, Telecommunication Engineering, and Naval Architecture (DITEN) of the University of Genoa has been carried out with several calibration and test targets. Moreover, simulations have been conducted using a finite-elements numerical solver in order to obtain the theoretical necessary coefficients for calibration methods.

Data processing and calibration procedures have been implemented through MATLAB scripts and obtained measurements and results have been reported. These results will be beneficial for current and future research in the field of subsurface imaging.

The future developments on the basis of this thesis will involve the study and test of other antenna calibration methods such as machine-learning based techniques, as well as the integration of calibration procedures with non-linear inversion algorithms, with numerical and experimental tests.

References

[1] M. Pastorino, *Microwave Imaging*, 1. edizione. Hoboken, NJ: John Wiley & Sons Inc, 2010.

[2] M. Pastorino y A. Randazzo, *Microwave Imaging Methods and Applications*. Artech House, 2018.

[3] R. Persico, *Introduction to Ground Penetrating Radar: Inverse Scattering and Data Processing*, 1. edizione. Piscataway, NJ: IEEE, 2014.

[4] N. K. Nikolova, *Introduction to Microwave Imaging*, 1st edition. Cambridge New Nork, NY Port Melbourne Delhi Singapore: Cambridge University Press, 2017.

[5] V. Schenone, C. Estatico, G. L. Gragnani, M. Pastorino, A. Randazzo, y A. Fedeli, «Microwave-Based Subsurface Characterization through a Combined Finite Element and Variable Exponent Spaces Technique», *Sensors*, vol. 23, n.º 1, Art. n.º 1, ene. 2023, doi: 10.3390/s23010167.

[6] A. Randazzo, C. Ponti, A. Fedeli, M. Pastorino, y G. Schettini, «A Hybrid Lebesgue-Space Inverse-Scattering Technique for Microwave Imaging of Objects Hidden Behind a Wall», en *2022 16th European Conference on Antennas and Propagation (EuCAP)*, mar. 2022, pp. 1-5. doi: 10.23919/EuCAP53622.2022.9769492.

[7] V. Schenone, A. Fedeli, C. Estatico, M. Pastorino, y A. Randazzo, «Experimental Assessment of a Novel Hybrid Scheme for Quantitative GPR Imaging», *IEEE Geosci. Remote Sens. Lett.*, vol. 19, pp. 1-5, 2022, doi: 10.1109/LGRS.2021.3121808.

[8] V. Schenone, A. Fedeli, C. Estatico, M. Pastorino, y A. Randazzo, «Assessment of a non-Hilbertian Inverse Scattering Approach for Electromagnetic Tomography in Subsurface Environments», en *2023 17th European Conference on Antennas and*

Propagation (EuCAP), mar. 2023, pp. 1-5. doi: 10.23919/EuCAP57121.2023.10133256.

[9] A. Fedeli, V. Schenone, M. Pastorino, y A. Randazzo, «An LSTM Based Strategy for Data and Model Calibration in Subsurface Electromagnetic Imaging», en *2022 IEEE Conference on Antenna Measurements and Applications (CAMA)*, dic. 2022, pp. 1-3. doi: 10.1109/CAMA56352.2022.10002550.

[10] V. Schenone, A. Fedeli, C. Estatico, M. Pastorino, y A. Randazzo, «Nonlinear Inversion for Microwave Characterization of Targets in Non-Homogeneous Media», en *2022 International Conference on Electromagnetics in Advanced Applications (ICEAA)*, sep. 2022, pp. 97-97. doi: 10.1109/ICEAA49419.2022.9899997.

[11] V. Schenone, A. Fedeli, M. Pastorino, A. Randazzo, y C. Estatico, «A Hybrid Qualitative-Quantitative Electromagnetic Imaging Method for Subsurface Prospecting», en *2022 IEEE International Conference on Imaging Systems and Techniques (IST)*, jun. 2022, pp. 1-6. doi: 10.1109/IST55454.2022.9827669.

[12] A. Fedeli, V. Schenone, M. Pastorino, y A. Randazzo, «Multistatic Electromagnetic Imaging of Dielectric Targets with LSTM Cells», en *2022 16th European Conference on Antennas and Propagation (EuCAP)*, mar. 2022, pp. 1-5. doi: 10.23919/EuCAP53622.2022.9769681.

[13] A. Randazzo *et al.*, «A Two-Step Inverse-Scattering Technique in Variable-Exponent Lebesgue Spaces for Through-the-Wall Microwave Imaging: Experimental Results», *IEEE Trans. Geosci. Remote Sens.*, vol. 59, n.º 9, pp. 7189-7200, sep. 2021, doi: 10.1109/TGRS.2021.3052608.

[14] V. Schenone, A. Fedeli, M. Pastorino, A. Randazzo, y C. Estatico, «Microwave Imaging of Dielectric Targets by Means of a Variable-Exponent Finite-Elements Approach», en *2021 IEEE Conference on Antenna Measurements & Applications (CAMA)*, nov. 2021, pp. 546-549. doi: 10.1109/CAMA49227.2021.9703641.

[15] A. Randazzo *et al.*, «Through-the-Wall Imaging by means of a Hybrid Inverse-Scattering Procedure», en *2021 XXXIVth General Assembly and Scientific Symposium of the International Union of Radio Science (URSI GASS)*, ago. 2021, pp. 1-3. doi: 10.23919/URSIGASS51995.2021.9560268.

[16] S. Lambot, E. C. Slob, I. van den Bosch, B. Stockbroeckx, y M. Vanclooster, «Modeling of ground-penetrating Radar for accurate characterization of subsurface electric properties», *IEEE Trans. Geosci. Remote Sens.*, vol. 42, n.º 11, pp. 2555-2568, nov. 2004, doi: 10.1109/TGRS.2004.834800.

[17] «Solve nonlinear least-squares (nonlinear data-fitting) problems - MATLAB lsqnonlin - MathWorks». https://es.mathworks.com/help/optim/ug/lsqnonlin.html?lang=en (accedido 28 de junio de 2023).

[18] «Solve system of linear equations — least-squares method - MATLAB lsqr - MathWorks España». https://es.mathworks.com/help/matlab/ref/lsqr.html (accedido 29 de junio de 2023).

Annex: Implemented code

Code of first calibration method, described in Section 2.1.1:

```
%Script for calibration by finding least squares solution of
%non-linear system

clear all; close all;

%FIRST PART: Obtain H,Hf,Hi by simulated and experimental values

%We collect data in Q dif positions for each f
Q = 8; %number of positions of calibration data
f = 1.45e9:10e6:2e9; %freqency vector (F=56)

%Importing VNA values

%Q rows (positions) and F columns (freqs)
S11_exp_target = ones(size(f,2),Q); %S11 in experimental case,
from VNA
for q = 1:Q

    filename_exp = sprintf('Example_exp_pos_%d.s1p',q-1);
    sobj_exp = sparameters(filename_exp);
    S11_exp_target(:,q) = sobj_exp.Parameters(:,:,46:101);

end

%Importing Simulation values

S11_theor = ones(size(f,2),Q); %S11 in theoretical case, from
simulations
for q = 1:Q

    filename_theor = sprintf('Example_theor_pos_%d.s1p',q-1);
    sobj_theor = sparameters(filename_theor);
    S11_theor(:,q) = sobj_theor.Parameters(:,:,:);
end

S11_theor = fliplr(S11_theor); %Flip the positions as in
simulations the order is inverse

%Final Hi,H,Hf vectors
Hi_vector = ones(1,size(f,2));
H_vector = ones(1,size(f,2));
Hf_vector = ones(1,size(f,2));

%Solve the system for each f
for i = 1:size(f,2)

    %Define the system of equations (Q equations)
    system = @(x)[...
    x(2) + ((x(1)*S11_theor(i,1))/(1 - x(3)*S11_theor(i,1))) -
S11_exp_target(i,1),...
    x(2) + ((x(1)*S11_theor(i,2))/(1 - x(3)*S11_theor(i,2))) -
S11_exp_target(i,2),...
```

```
    x(2) + ((x(1)*S11_theor(i,3))/(1 - x(3)*S11_theor(i,3))) -
S11_exp_target(i,3),...
    x(2) + ((x(1)*S11_theor(i,4))/(1 - x(3)*S11_theor(i,4))) -
S11_exp_target(i,4),...
    x(2) + ((x(1)*S11_theor(i,5))/(1 - x(3)*S11_theor(i,5))) -
S11_exp_target(i,5),...
    x(2) + ((x(1)*S11_theor(i,6))/(1 - x(3)*S11_theor(i,6))) -
S11_exp_target(i,6),...
    x(2) + ((x(1)*S11_theor(i,7))/(1 - x(3)*S11_theor(i,7))) -
S11_exp_target(i,7),...
    x(2) + ((x(1)*S11_theor(i,8))/(1 - x(3)*S11_theor(i,8))) -
S11_exp_target(i,8)];

    x0 = [0,0,0]; %Initial point
    options =
optimoptions(@lsqnonlin,'MaxFunctionEvaluations',500,'FunctionTole
rance',1e-3);
    x = lsqnonlin(system,x0,[],[],options);

    H_vector(i) = x(1);
    Hi_vector(i) = x(2);
    Hf_vector(i) = x(3);

end

figure;
subplot(2,1,1);
plot(f,abs(Hi_vector));
ylabel('|Hi|');
xlabel('f(Hz)');
title('abs(Hi)');
subplot(2,1,2);
plot(f,angle(Hi_vector));
title('angle(Hi)');
ylim([-pi,pi]);
ylabel('angle(Hi)');
xlabel('f(Hz)');

figure;
subplot(2,1,1);
plot(f,abs(Hf_vector));
title('abs(Hf)');
ylabel('|Hf|');
xlabel('f(Hz)');
subplot(2,1,2);
plot(f,angle(Hf_vector));
title('angle(Hf)');
ylim([-pi,pi]);
ylabel('angle(Hf)');
xlabel('f(Hz)');

figure;
```

```
subplot(2,1,1);
plot(f,abs(H_vector));
title('abs(H)');
ylabel('|H|');
xlabel('f(Hz)');
subplot(2,1,2);
plot(f,angle(H_vector));
title('angle(H)');
ylim([-pi,pi]);
ylabel('angle(H)');
xlabel('f(Hz)');


%SECOND PART: Calibrate experimental measurements with Hf,H,Hi

%Importing VNA values to calibrate with the obtained TF
Q = 34; %Number of positions of test data
S11_exp_target = ones(size(f,2),Q); %S11 values with target
S11_exp_without = ones(size(f,2),Q); %S11 values without target

for q = 1:Q

    filename_without = sprintf('Example_without_pos_%d.s1p',q-1);
    filename_target = sprintf('Example_target_pos_%d.s1p',q-1);

    sobj_target = sparameters(filename_target);
    sobj_without = sparameters(filename_without);
    S11_exp_target(:,q) = sobj_target.Parameters(:,:,46:101);
    S11_exp_without(:,q) = sobj_without.Parameters(:,:,46:101);

end

%Save values before calibration for comparison
S11_before_calibration_target = S11_exp_target;
S11_before_calibration_without = S11_exp_without;

S11_calibrated_target = ones(size(f,2),Q);
S11_calibrated_without = ones(size(f,2),Q);

%Loop where calibration equation is applied
for q = 1:Q
    for fi = 1:size(f,2)
        S11_calibrated_target(fi,q) = (S11_exp_target(fi,q) -
Hi_vector(fi))/...
            (Hf_vector(fi)*S11_exp_target(fi,q) -
Hf_vector(fi)*Hi_vector(fi) + H_vector(fi));
        S11_calibrated_without(fi,q) = (S11_exp_without(fi,q) -
Hi_vector(fi))/...
            (Hf_vector(fi)*S11_exp_without(fi,q) -
Hf_vector(fi)*Hi_vector(fi) + H_vector(fi));
    end
end
```

```
%THIRD PART: Obtain BScan

% frequencies defined in f: fc = 1.45e9 to 2GHz
pts = size(f,2); %Number of frequencies
df = f(2) - f(1); %Frequency gap
fst = floor(f(1)/df);

N = 4096; %fft points
signal_td_target = zeros(N,Q);
signal_td_without = zeros(N,Q);

for q = 1:Q

    %pts is the number of samples, here we are adding zeros from
0Hz to
    %1GHz to perform the fft
    s11_fd_target = zeros(fst + pts,1);
    s11_fd_target(fst+1:fst+pts) = S11_calibrated_target(:,q);

    s11_fd_without = zeros(fst + pts,1);
    s11_fd_without(fst+1:fst+pts) = S11_calibrated_without(:,q);

    %Performing fft
    s11_td_target = ifft(s11_fd_target, N, 'symmetric');
    signal_td_target(:,q) = s11_td_target;

    s11_td_without = ifft(s11_fd_without, N, 'symmetric');
    signal_td_without(:,q) = s11_td_without;

end

%dt is 1/df, the time gap
dt = 1/df;
time = linspace(0,dt,N);
position = linspace(11,44,Q); %x-axis, position in lab

%Cutting matrix to adjust the desired time visualization
time_limit = 10e-9;
time_limit_index = find(time <= time_limit);
time = time(time_limit_index);
time_limit_index = time_limit_index(size(time_limit_index,2));

% Total field
figure;
imagesc(position,time,signal_td_target(1:time_limit_index,:));
colorbar;
title('Total field after calibration (First method)');
ylabel('t(s)');
xlabel('Position from lab origin (cm)');
```

```
%Scattered field
figure;
imagesc(position,time,signal_td_target(1:time_limit_index,:)...
    - signal_td_without(1:time_limit_index,:));
colorbar;
title('Scattered field after calibration (First method)');
ylabel('t(s)');
xlabel('Position from lab origin (cm)');

%Analogous process with values before calibration

S11_exp_target = S11_before_calibration_target;
S11_exp_without = S11_before_calibration_without;

% frequencies and select from fc = 1.45e9 to 2GHz
freq = linspace(1.45e9,2e9,56);
pts = size(freq,2);

df = freq(2) - freq(1);
fst = floor(freq(1)/df);

signal_td_before_calibration_target = zeros(N,Q);
signal_td_before_calibration_without = zeros(N,Q);
for q = 1:Q

    s11_fd_target = zeros(fst + pts,1);
    s11_fd_target(fst+1:fst+pts) = S11_exp_target(:,q);
    s11_td_target = ifft(s11_fd_target, N, 'symmetric');
    signal_td_before_calibration_target(:,q) = s11_td_target;

    s11_fd_without = zeros(fst + pts,1);
    s11_fd_without(fst+1:fst+pts) = S11_exp_without(:,q);
    s11_td_without = ifft(s11_fd_without, N, 'symmetric');
    signal_td_before_calibration_without(:,q) = s11_td_without;

end

%dt is 1/df, the time gap
dt = 1/df;
position = linspace(11,44,Q); %x-axis, position in lab

% Total field before calibration
figure;
imagesc(position,time,signal_td_before_calibration_target(1:time_l
imit_index,:));
colorbar;
title('Total field before calibration');
ylabel('t(s)');
xlabel('Position from lab origin (cm)');

%Scattered field before calibration
figure;
```

```
imagesc(position,time,signal_td_before_calibration_target(1:time_l
imit_index,:)...
    - signal_td_before_calibration_without(1:time_limit_index,:));
colorbar;
title('Scattered field before calibration');
ylabel('t(s)');
xlabel('Position from lab origin (cm)');
```

Code of second calibration method, described in Section 2.1.2:

```
%Script used for calibration assuming Hi as the f.s. transfer
function of
%the antenna
clear all; close all;

%FIRST PART: Obtain Hi by performing a Time Gating

% read sp1 file (measured data)
filename = sprintf('Example_freespace_pos_0.s1p');
sobj = sparameters(filename);

%create vector with s11 values in free space
S11_exp_fs(1,:) = sobj.Parameters(:,:,:);
freq = sobj.Frequencies';

pts = size(freq,2); %number of frequencies used
df = freq(2) - freq(1);
fst = floor(freq(1)/df);
N = 4096; %fft points

% pts is the number of samples, here we are adding zeros from 0Hz
to 1GHz
s11_fd = zeros(fst + pts,1);
s11_fd(fst+1:fst+pts) = S11_exp_fs(1,:)';
s11_td = ifft(s11_fd, N, 'symmetric');

%dt is 1/df, the time gap
dt = 1/df;
time = linspace(0,dt,N);

%Time gating
time_floor = 26.67e-9; %Time at which is the wall reflection
indexes = find(time<=time_floor);
cutoff_time = time(indexes);
s11_td_cut = s11_td (indexes);

Hi = fft(s11_td_cut,N);
Hi_positive = Hi(1:N/2);
Hi_free_space = Hi_positive(101:301);

%SECOND PART: Obtain Hf and H solving the system of equations in a
matrix
%form

%We collect data in Q dif positions for each f
Q = 8; %number of positions
f = 1.45e9:0.01e9:2e9; %freq vector (F=56)

%Hi is known, we take only from 1.45 GHz to 2 GHz
Hi = Hi_free_space(46:101);

%Final H,Hf vectors
```

```
H_vector = zeros(size(f,2),1);
Hf_vector = zeros(size(f,2),1);

%Importing exp and simulation values and create matrix A and y
A = zeros(Q,2);
y = zeros(Q,1);

for i = 1:size(f,2)

    for q = 1:Q
    %Load data of Q positions for f in A and y
        filename_exp = sprintf('Example_exp_pos_%d.s1p',q-1);
        filename_sim = sprintf('Example_sim_pos_%d.s1p',8-q);

        sobj_exp = sparameters(filename_exp);
        S11_exp = squeeze(sobj_exp.Parameters(:,:,46:101));
        sobj_sim = sparameters(filename_sim);
        S11_sim = squeeze(sobj_sim.Parameters(:,:,:));

        %Defining matrix
        A(q,:) = [S11_sim(i)*(Hi(i) - S11_exp(i)), -S11_sim(i)];
        y(q) = Hi(i) - S11_exp(i);

    end

    %Obtain Hf(f) and H(f)
    x = lsqr(A,y,0.8);
    Hf_vector(i) = x(1);
    H_vector(i) = x(2);

end

figure;
subplot(2,1,1);
plot(f,abs(Hf_vector));
title('abs(Hf)');
ylabel('|Hf|');
xlabel('f(Hz)');
subplot(2,1,2);
plot(f,angle(Hf_vector));
title('angle(Hf)');
ylabel('angle(Hf)');
xlabel('f(Hz)');

figure;
subplot(2,1,1);
plot(f,abs(H_vector));
title('abs(H)');
ylabel('|H|');
xlabel('f(Hz)');
subplot(2,1,2);
plot(f,angle(H_vector));
```

```
title('angle(H)');
ylabel('angle(H)');
xlabel('f(Hz)');

figure;
subplot(2,1,1);
plot(f,abs(Hi));
title('abs(Hi)');
ylabel('|Hi|');
xlabel('f(Hz)');
subplot(2,1,2);
plot(f,angle(Hi));
title('angle(Hi)');
ylabel('angle(Hi)');
xlabel('f(Hz)');

%THIRD PART: Calibrate experimental measurements with Hf,H,Hi
Hi_vector = Hi;

%Importing VNA values to calibrate with the obtained TF
Q = 34;
S11_exp = ones(size(f,2),Q);
for q = 1:Q

    %Without target
    filename_without = sprintf('Example_without_pos_%d.s1p',q-1);
    %With target
    filename_target = sprintf('Example_target_pos_%d.s1p',q-1);

    sobj_without = sparameters(filename_without);
    S11_exp_without(:,q) = sobj_without.Parameters(:,:,46:101);
    sobj_target = sparameters(filename_target);
    S11_exp_target(:,q) = sobj_target.Parameters(:,:,46:101);
end

%Values before calibration to compare
S11_before_calibration_target = S11_exp_target;
S11_before_calibration_without = S11_exp_without;

S11_calibrated_target = ones(size(f,2),Q);
S11_calibrated_without = ones(size(f,2),Q);
%Loop where calibration equation is applied
for q = 1:Q
    for fi = 1:size(f,2)
        S11_calibrated_target(fi,q) = (S11_exp_target(fi,q) -
Hi_vector(fi))/...
            (Hf_vector(fi)*S11_exp_target(fi,q) -
Hf_vector(fi)*Hi_vector(fi) + H_vector(fi));
        S11_calibrated_without(fi,q) = (S11_exp_without(fi,q) -
Hi_vector(fi))/...
            (Hf_vector(fi)*S11_exp_without(fi,q) -
Hf_vector(fi)*Hi_vector(fi) + H_vector(fi));
```

```
    end
end


%FOURTH PART: Obtain BScan

S11_exp_target = S11_calibrated_target;
S11_exp_without = S11_calibrated_without;

% frequencies and select from fc = 1.45e9 to 2GHz
freq = linspace(1.45e9,2e9,56);
pts = size(freq,2); %number of freqs
N = 4096; %fft points
df = freq(2) - freq(1); %frequency gap
fst = floor(freq(1)/df);

signal_td_after_calibration_target = zeros(N,Q);
signal_td_after_calibration_without = zeros(N,Q);

%dt is 1/df, the time gap
dt = 1/df;
time = linspace(0,dt,N);
position = linspace(11,44,Q); %x-axis, position in lab

%Time limitation to desired visualization
time_limit = 10e-9;
time_limit_index = find(time <= time_limit);
time = time(time_limit_index);
time_limit_index = time_limit_index(size(time_limit_index,2));

for q = 1:Q

    % pts is the number of samples, here we are adding zeros from
0Hz to 1GHz
    s11_fd_target = zeros(fst + pts,1);
    s11_fd_target(fst+1:fst+pts) = S11_exp_target(:,q);
    s11_fd_without = zeros(fst + pts,1);
    s11_fd_without(fst+1:fst+pts) = S11_exp_without(:,q);

    %Applying ifft
    s11_td_target = ifft(s11_fd_target, N, 'symmetric');
    signal_td_after_calibration_target(:,q) = s11_td_target;
    s11_td_without = ifft(s11_fd_without, N, 'symmetric');
    signal_td_after_calibration_without(:,q) = s11_td_without;

end

% Total field
figure;
imagesc(position,time,signal_td_after_calibration_target(1:time_li
mit_index,:));
colorbar;
```

```
colorbar;
title('Total field after calibration (Method of Hi known)');
ylabel('t(s)');
xlabel('Position from lab origin (cm)');

%Scattered field
figure;
imagesc(position,time,signal_td_after_calibration_target(1:time_li
mit_index,:)...
    - signal_td_after_calibration_without(1:time_limit_index,:));
colorbar;
title('Scattered field after calibration (Method of Hi known)');
ylabel('t(s)');
xlabel('Position from lab origin (cm)');

%With values before calibration

S11_exp_target = S11_before_calibration_target;
S11_exp_without = S11_before_calibration_without;

% frequencies and select from fc = 1.45e9 to 2GHz
freq = linspace(1.45e9,2e9,56);
pts = size(freq,2);
df = freq(2) - freq(1);
fst = floor(freq(1)/df);

signal_td_before_calibration_target = zeros(N,Q);
signal_td_before_calibration_without = zeros(N,Q);
for q = 1:Q

    % pts is the number of samples, here we are adding zeros from
0Hz to 1GHz
    s11_fd_target = zeros(fst + pts,1);
    s11_fd_target(fst+1:fst+pts) = S11_exp_target(:,q);
    s11_fd_without = zeros(fst + pts,1);
    s11_fd_without(fst+1:fst+pts) = S11_exp_without(:,q);

    %Applying ifft
    s11_td_target = ifft(s11_fd_target, N, 'symmetric');
    signal_td_before_calibration_target(:,q) = s11_td_target;
    s11_td_without = ifft(s11_fd_without, N, 'symmetric');
    signal_td_before_calibration_without(:,q) = s11_td_without;

end

%dt is 1/df, the time gap
dt = 1/df;
position = linspace(11,44,Q); %x-axis, position in lab

% Total field before calibration
figure;
```

```
imagesc(position,time,signal_td_before_calibration_target(1:time_l
imit_index,:));
colorbar;
title('Total field before calibration (Method with Hi known)');
ylabel('t(s)');
xlabel('Position from lab origin (cm)');

%Scattered field before calibration
figure;
imagesc(position,time,signal_td_before_calibration_target(1:time_l
imit_index,:)...
    - signal_td_before_calibration_without(1:time_limit_index,:));
colorbar;
title('Scattered field before calibration (Method of Hi known)');
ylabel('t(s)');
xlabel('Position from lab origin (cm)');
```